AN ABSTRACT OF THE THESIS OF

Utpal Das for the degree of Master of Science in Electrical and Computer Engineering presented on Dec. 9, 1983.

Title: Some Transport Properties of Organometallic VPE $Al_xGa_{1-x}As$ and Ion-implanted GaAs

Redacted for Privacy

Abstract approved: Pallab K. Bhattacharya

Temperature-dependent measurements in the range $20 \leq T(K) \leq 600$ have been made on undoped and Si-doped organometallic vapour phase epitaxial $Al_xGa_{1-x}As$. Data obtained from Hall and high-field measurements using the probe technique have been analysed. The transport parameters in the samples have been obtained from analysis of data and the relative importance of the various scattering mechanisms in different composition ranges have been elucidated. It was found that space charge scattering plays an important role in limiting electron mobility at 300 K for $0 < x \leq 0.3$, and intervalley scattering plays the dominant role in the composition range $0.3 \leq x \leq 0.5$. Donor levels, with their activation energy E_D increasing with x upto 0.113 eV at x = 0.35, are present in the undoped samples. The dominant donor level in the Si-doped samples also exhibits a similar trend, with E_D = 0.095 eV for x = 0.35. High values of drift velocity in samples with $x \geq 0.4$ at 300 K and similar features observed in some samples

with $x < 0.4$ at high temperatures have been attributed to electron transfer from the substrate to the epitaxial layers.

A detailed analysis of the data obtained from Hall measurements in the temperature range $12 \leq T$ (K) < 300 has been done on Si-implanted and annealed GaAs layers. The highest room-termperature mobility observed is 2900 $cm^2/V.s$. Although an analysis of the Hall mobility data shows a high dopant concentration ($\sim 10^{17}$ cm^{-3}), a poor electrical activation of the dopants ($\sim$4.5 - 14.8%) has been measured.

An anomalous increase of the measured Hall carrier concentration at very low temperatures has been observed in both OMVPE $Al_xGa_{1-x}As$ and Si-implanted semi-insulating GaAs layers. The phenomena is not clearly understood.

Some Transport Properties of Organometallic Vapour Phase Epitaxial $Al_xGa_{1-x}As$ and Ion-Implanted GaAs

by

Utpal Das

A THESIS

submitted to

Oregon State University

in partial fulfillment of
the requirements for the
degree of

Master of Science

Completed December 9, 1983

Commencement June, 1984

APPROVED:

Redacted for Privacy

Associate Professor of Electrical and Computer Engineering

Redacted for Privacy

Chairman of department of Electrical and Computer Engineering

Redacted for Privacy

Dean of Graduate School

Date thesis is presented December 9, 1983

Typed by Cheryl Richards for Utpal Das

Acknowledgement

In submitting this report I have the opportunity to express my deepest sense of gratitude to my major professor, Dr. P.K. Bhattachanya (Associate Professor, Department of Electrical and Computer Engineering, Oregon State University) for his constant co-operation and advice.

I also express my thanks to the authorities of Solid State Laboratories (Varian Associates) for providing me with the $Al_xGa_{1-x}As$ samples needed for the work. Thanks are also due to M/S ITT for their partial support, financially and in providing me with the Ion-implanted GaAs samples.

Partial support has also been provided by the Department of Office of Basic Energy Sciences, under the contract DE-AT06-81ER10939. I acknowledge their support with due regards.

I am also grateful to Dr. S. Subramanian, Post Doctoral Research Fellow in this department, for his meaningful suggestions and helpful discussions from time to time.

I must acknowledge the advice and help extended to me by Mr. P. Banerjee and Mr. M.V. Rao on quite a few occasions.

Finally, I wish to thank Prof. C. Drake, Prof. J. Owen, Prof. V.K. Tripathi and Prof. R. Rathja who spared their valuable time and helped me form my graduate committee.

Utpal Das

Department of Electrical
and Computer Engineering,
Oregon State University,
Corvallis, Oregon 97331
November 28, 1983

TABLE OF CONTENTS

INTRODUCTION 1

MULTIVALLEY TRANSPORT IN SEMICONDUCTORS. 5

EXPERIMENTAL TECHNIQUES. 22

TRANSPORT AND ASSOCIATED EFFECTS IN ION-IMPLANTED GaAs 30

LOW AND HIGH FIELD TRANSPORT IN $Al_xGa_{1-x}As$ 38

CONCLUSION 64

BIBLIOGRAPHY 66

APPENDICES 70

I PROGRAM FOR MOBILITY ANALYSIS OF Si-IMPLANTED GaAs. . . . 70

II PROGRAM FOR MOBILITY ANALYSIS OF $Al_xGa_{1-x}As$ IN A WIDE RANGE OF ALLOYING COMPOSITIONS. 74

III PROGRAM FOR THE HALL CONCENTRATION ANALYSIS OF $Al_xGa_{1-x}As$. 80

LIST OF FIGURES

Figure		Page
2.1	Band Structure (E-k diagram) for GaAs	6
2.2	Conduction bond structure in $Al_xGa_{1-x}As$ as determined from earlier work	6
2.3	TO and LO mode frequencies plotted versus alloy composition for AlAs and GaAs	14
2.4	Simplified picture of the velocity field characteristic in the bridge region of the H-device	20
2.5	a) H-device geometry b) Expected field distribution	20
2.6	A simplified picture of the current-voltage characteristic of a complete H-device	20
3.1	Flowchart for preperations of Hall samples and Hall measurement	23
3.2	Mounting of the sample on the cryostat	25
3.3	Flowchart for the preparation of H-devices and measurement of high-field mobility	27
3.4	Measurement setup for high-field mobility	28
4.1	Measured variation of the Hall mobility with temperature for Si-implanted GaAs samples	31
4.2	Measured variation of the Hall mobility with temperature for Si-implanted GaAs samples	32
4.3	Measured variation of the sheet carrier concentration with temperature for the Si-implanted GaAs samples from Hall measurement	33
4.4	Values of the mobilities limited by different scattering mechanisms for a Si-implanted GaAs sample. The total mobility exactly coencides with the data (in small dots)	34
4.5	Technique tried to find the mobility in different regions of the implanted layer	36

LIST OF FIGURES (cont.)

Figure		Page
5.1	Measured variation of Hall mobility with temperature in undoped OMVPE $Al_xGa_{1-x}As$ for different alloy compositions	39
5.2	Measured variation of Hall mobility with composition at 300 K in undoped OMVPE $Al_xGa_{1-x}As$	40
5.3	Temperature dependence of Hall electron mobility, and sheet electron concentration, n_s, in OMVPE $Al_{0.4}Ga_{0.6}As$	41
5.4	Variation of Hall mobility with temperature in undoped OMVPE $Al_{0.1}Ga_{0.9}As$	43
5.5	Variation of Hall mobility with temperature in undoped OMVPE $Al_{0.25}Ga_{0.75}As$	43
5.6	Electron mobilities limited by the different relevant scattering mechanisms in Γ and X minima in $Al_{0.4}Ga_{0.6}As$	44
5.7	Measured variation of Hall electron concentration with composition at 300 K in undoped OMVPE $Al_xGa_{1-x}As$	45
5.8	Measured and calculated variations of Hall electron concentration with temperature in undope $Al_xGa_{1-x}As$ samples	47
5.9	Measured and calculated variations of Hall electron concentration with temperature in Si-doped $Al_xGa_{1-x}As$ samples	47
5.10	Measured variation of Hall electron concentration for undoped $Al_xGa_{1-x}As$ samples over a wide range of temperatures	48
5.11	Variation of the Hall concentration for photohall measurement with undoped $Al_{0.25}Ga_{0.75}As$	49
5.12	Measured and calculated variations of Hall electron concentration with temperature in undoped $Al_xGa_{1-x}As$ samples	50

LIST OF FIGURES (cont.)

Figure		Page
5.13	The data points for the energy position of the L minima and the donor levels determined in this study	51
5.14	Ratio of mobilities limited by alloy and space-charge scattering	56
5.15	Mobilities in Γ and X valleys limited by alloy, space charge and intervalley scattering in OMVPE $Al_xGa_{1-x}As$	58
5.16	Velocity-field characteristics of electrons in OMVPE $Al_xGa_{1-x}As$ with $0 < x \leqslant 0.4$	59
5.17	Potential distribution along the bridge of an H-device, fabricated on OMVPE $Al_{0.4}Ga_{0.6}As$	60
5.18	Velocity-field characteristic of electrons in OMVPE $Al_{0.25}Ga_{0.75}As$ at 300 K and 400 K	61
5.19	Process by which there is real-space electron transfer from the 2DEG to the $Al_xGa_{1-x}As$ epilayer at high applied electric fields	62
5.20	Effect of probe loading	62

LIST OF TABLES

Table		Page
1-1	Comparison of epitaxial growth techniques	2
3-1	Summary of the metallization and alloying process for the fabrication of ohmic contacts	24
4-1	Summary of parameters used for analysis for Si-implanted GaAs	36
4-2	Characteristics of Si-implanted GaAs from analysis of Hall data	37
5-1	Summary of parameters used for analysis of OMVPE $Al_xGa_{1-x}As$ Hall data	53
5-2	Summary of the measured data for OMVPE $Al_xGa_{1-x}As$ samples	54
5-3	Characteristics of undoped and Si-doped OMVPE $Al_xGa_{1-x}As$ obtained from analysis of Hall data	55

LIST OF SYMBOLS FREQUENTLY USED

q	Electronic charge
m^*	Effective mass of the carrier
π	Constant (3.142)
N_N	Total number of impurities per unit volume in the semiconductor
$\hbar$	Reduced Plank's Constant
k_o	Boltzman Constant
T	Temperature in degrees Kelvin
m_o	Free carrier mass
ϵ_s	Static dielectric constant fo the Semiconductor
τ	Relaxation time for scattering
N_D	Concentration of donor impurities
N_A	Concentration of acceptor impurities
n^*	Effective screening density
ρ	Mass density of the semiconductors
w_ℓ	Longitudinal sound velocity in the semiconductor
E_1	Acoustic deformation potential
e_{14}	Piezoelectric constant
C_t	Average transverse elastic constant
C_1	Average longitudinal elastic constant
ϵ_d	High frequency dielectric constant of the semiconductor
θ	Polar Optical Phonon temperature of the semiconductor
$G(\frac{\theta}{T})$	Fortini's function
N_s	Concentration of space charge
A	Effective scattering area of the space charge region

LIST OF SYMBOLS FREQUENTLY USED (cont.)

x	Percentage of alloying in (Al,Ga)As
ΔU	Alloy scattering potential
N_j	Number of equivalent minima for either X or L valleys
ΔE_{ij}	Intervalley separation of energies
D_{ij}	Coupling coefficients for intervalley scattering
m_t	Transverse effective mass of carriers
m_l	Longitudinal effective mass of carriers
E	Energy of a carrier
J	Current density
I	Current
V	Voltage
ϑ	Velocity
μ	Mobility
n	Effective carrier concentration
ε	Electronic field
σ	Electrical conductivity

Some Transport Properties of Organometallic
Vapour Phase Epitaxial $Al_xGa_{1-x}As$ and Ion-Implanted GaAs

Chapter 1

Introduction

In recent years the $Al_xGa_{1-x}As$ alloys have attracted attention for device applications because of the minimal lattice mismatch (~0.16%) between GaAs and AlAs [1]. The growth of GaAs—(Al,Ga)As heterostructures is of particular interest for the fabrication of many devices, such as lasers [2], photocathodes [3], microwave FETs [4], and solar cells [5]. Quantum-Well-Heterostructures (QWH), alternating thin layers of GaAs and $Al_xGa_{1-x}As$, are also of current interest. Significant properties include laser operation above the bluk GaAs band edge and the demonstration of high electron mobilities in these hetrostructures.

The organometallic vapour phase epitaxial (OMVPE) growth technique, which is basically an irreversible pyrolysis of group III metal alkyl vapours in a stream of group V hydrides on a heated substrate, has several unique advantages: (a) capability of large area growth like SiO_2 deposition; (b) small autodoping because of the low temperatures used for growth and (c) precise thickness controlability of thin films. The OMVPE growth technique is now being used widely for the growth of GaAs, $Al_xGa_{1-x}As$ and other mixed alloys. In particular the technique allows the growth of uniform QWH structures having a large number of thin epitaxial layers with the necessary abrupt interfaces between layers [6]. Table 1-1 compares the relative advantages and disadvantages of various growth techniques.

TABLE 1-1
Comparison of epitaxial growth techniques.

Technique	Characteristic				
	Solid composition	Purity	Inherent advantages	Inherent disadvantages	Status
LPE	Thermodynamics (phase diagram)	III melt container, *gettering*	Simple, *high purity*	Volume limited, inflexible morphology	Laboratory technique
VPE (hydride)	Thermodynamics	Gases, leaks, reactor materials	Flexible, large scale	No AlGaAs or other Al alloys	Production technique (GaAsP)
OMVPE	Kinetics, arrival at surface	OM sources AsH_3, C contamination, leaks	*Most versatile*, large scale (?) simple	C contamination, problems with In (?)	Potential commercial AlGaAs
MBE	Kinetics, flux, sticking coefficient	Vacuum sources, system (walls)	Most abrupt (2--10 A), low temperature	Expensive, slow growth rate, problems with phosphorus	Special structures

After G.B. Stringfellow [75]

For the proper understanding of device behavior it is necessary to characterize and understand the material properties. Early studies on OMVPE $Al_xGa_{1-x}As$ were reported by Stringfellow et al [8-11], Wagner et al [12, 13], Hallais et al [14], and Johnson et al [15]. Photoluminescence capacitance spectroscopy and Hall measurements performed by these authors were mainly confined to direct band gap crystals. Later work by Matsumoto and others [16] has revealed that n-type OMVPE $Al_xGa_{1-x}As$ with $0 < x \leqslant 0.5$ and thermal activation energies ΔE_T of 0.82, 0.62 and 0.38 exibit invariant ΔE_T, decreasing thermal capture crossection and increasing thermal barrier energy with increasing Al content. The concentration of the first two shallower traps increase with Al-content also. Their work also indicated the presence of a band of states near the grown $GaAs/Al_xGa_{1-x}As$ interface region. For the first time it was shown by Matsumoto et al [17] that transfer doping effects at the interface of OMVPE $Al_xGa_{1-x}As$ grown on semi-insulating GaAs: Cr leads to high electron mobilities.

The purpose of this work was to make a detailed investigation of low and high field transport properties of high-purity and Si- doped n-type OMVPE $Al_xGa_{1-x}As$ alloys. Measurements were also made to gain a better understanding of the epilayer-substrate interface.

Recent progress in ion-implantation as a means of controlled doping of elemental and compound semi-conductors have led to significant advantages in the technology and fabrication of integrated circuits (IC). Implantation of high-energy donor ions into semi-insulating GaAs and subsequent thermal or laser annealing produces n-type active layers whose thickness and carrier concentration can be

controlled by the implant dose and energy. Deep level defects induced by the implant-and-anneal procedure can produce detrimental effects in the performance of FETs and similar devices. Some results on deep levels in Si-implanted annealed GaAs: Cr [18, 19, 20] have been reported, but no detailed studies have been made. A recent report by Bhattacharya et al [21] has shown that in Si-implanted semi-insulating GaAs layers the presence of (Si_{Ga} - Si_{As}) pair complexes can explain, qualitatively, the poor electrical activation for high Si implant doses in GaAs. A detailed study of the transport properties in such Si-implanted and annealed GaAs layers has been made to determine the compensation and scattering processes in the material and to evaluate the properties of the implanted layer--substrate interface.

Chapter 2

Multi-Valley Transport in Semiconductors

$Al_xGa_{1-x}As$ is a solid solution of GaAs and AlAs. Thus the band structure of $Al_xGa_{1-x}As$ may be taken as intermediate between those of GaAs (Fig 2.1) and AlAs, both having sphalerite crystal structures. As has been reported by Saxena et al [22-25] the three conduction band Γ, L, X model for $Al_xGa_{1-x}As$ fits well with the experimental data. The varying conduction band structure as a function of alloy composition plays a critical role in determining the transport properties. The conduction band structure determined by the earlier work of Saxena and others [26] is shown in Fig 2.2.

2.1 Low-field transport

To analyse the mobility data the following assumptions are usually made: (a) the back scattering process has a characteristic relaxation time $\tau(E)$ where E is the electron energy in k_oT.(b) the electrons are scattered in a parabolic band and, (c) the various scattering mechanisms are independent of each other. It might be noted that the last assumption may not be strictly valid since the electron-phonon interaction could take place while the electron's motion is influenced by the potential of an ionized impurity. Also a true relaxation time cannot be defined for electron scattering by polar optical modes [27].

For low ($0 \leqslant x \lesssim 0.3$) and high ($0.6 \lesssim x \leqslant 1.0$) AlAs content, the temperature dependence ($15 \lesssim T \lesssim 300K$) of μ_H has been successfully explained by a single conduction band model [28]. In the intermediate composition range where the conduction crossovers take place the

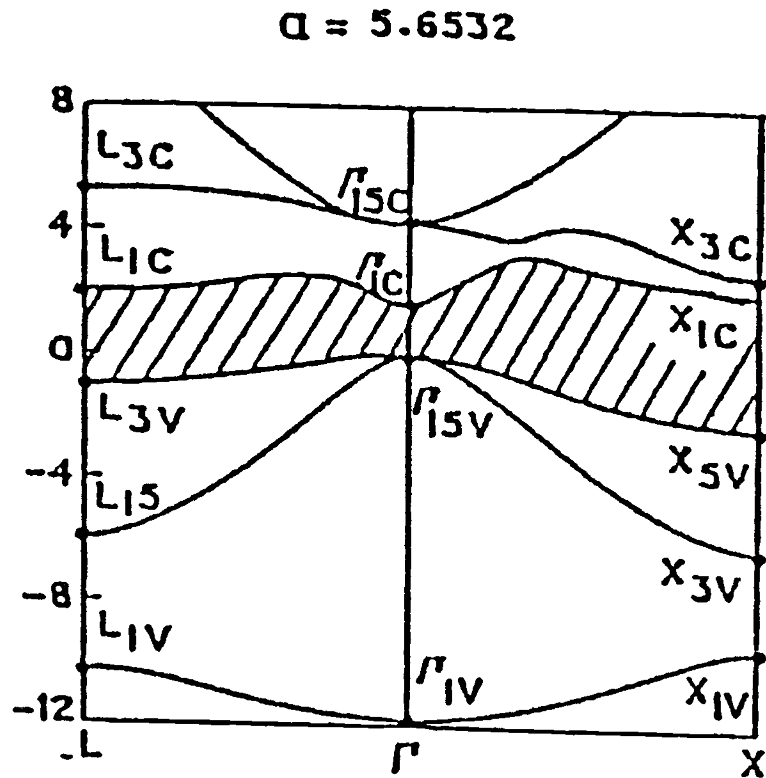

Fig 2.1 Band structure (E-k diagram) for GaAs (Ref [31]).

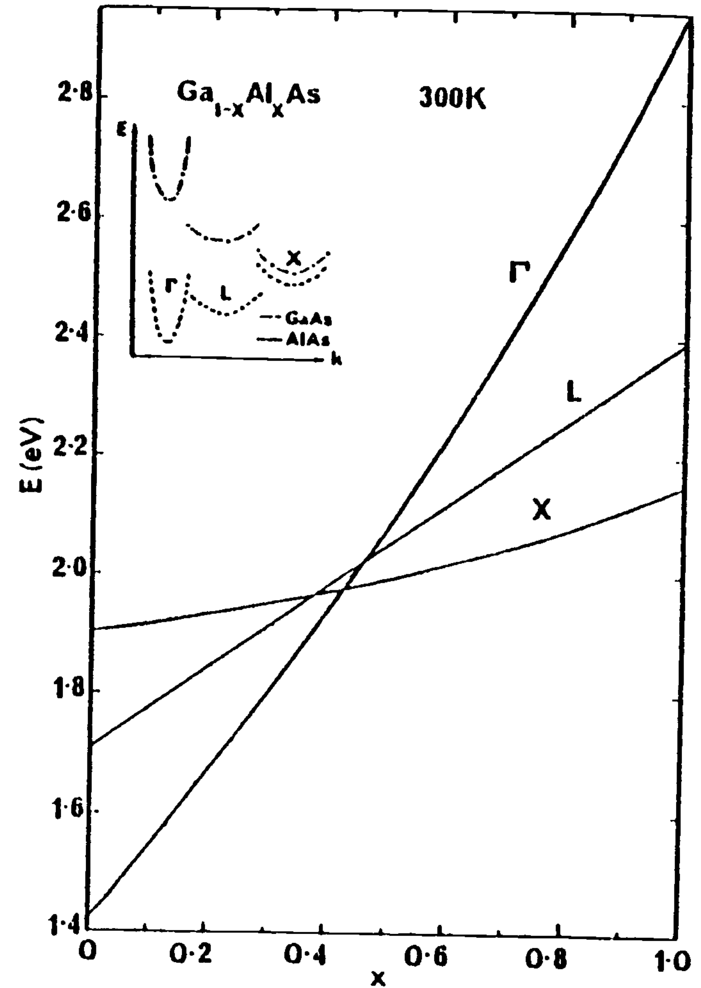

Fig 2.2 Conduction band structure in $Al_xGa_{1-x}As$ as determined from earlier work (see text).

variation of mobility was only partially analysed by Saxena [28] because some of the parameters required for the analysis were still unknown.

The impurity atoms provide energy levels in the forbidden gap, and these levels are occupied by electrons (for donor atoms) and are empty (for acceptor atoms) at very low temperatures. The collision process at very low temperatures occurs between neutral impurity atoms. The treatment of neutral impurity scattering developed by Erginsoy [29] and later modified by Sclar [30] is yet not fully understood [31].

Using Sclar's equation

$$\mu_{NI} = \frac{2q\ m^{*\frac{1}{2}}\ |E_N|^{\frac{1}{2}}}{\sqrt{2}\ \pi^{3/2}\ N_N\ \hbar^2} \left[\frac{2}{3} \left(\frac{k_oT}{E_N}\right)^{\frac{1}{2}} + \frac{1}{3} \left(\frac{E_N}{k_oT}\right)^{\frac{1}{2}} \right] \qquad (1)$$

where $E_N = \left[\frac{0.71\ (m^*/m_o)}{\epsilon_s^2}\right]$ in e.V. (2)

and N_N is the total number of impurities, m_o is the free carrier mass, m^* is the effective mass of the carrier, ϵ_s is the static dielectric constant in the semiconductor, q is the charge of the carriers, k_o is the Boltzman constant, $\hbar$ is the reduced Plank's constant and T is the temperature in degrees Kelvin.

It has been seen that for $T \geqslant 20K$ the effects of neutral impurity scattering becomes negligibly small compared to other scattering mechanisms.

With increasing temperature the collision process is dominated by the collisions of electrons with ionised impurity atoms. Since the

charged impurity atoms cannot scatter high energy electrons, the effect of ionised impurities decreases as the temperature is increased. However, in compound semiconductors grown by current epitaxy techniques, the concentration of impurity atoms are usually large and ionised impurities dominate the collision process even at $T \geqslant 77K$. The scattering by ionised impurities is therefore considered an important collision process for compound semiconductors.

The scattering of electrons by singly ionized impurities is described by the Brooks-Herring equation [32, 33] which takes into account the screening potential of the ionised waters. The ionised impurity scattering limited mobility is

$$\mu_I = \frac{3.28 \times 10^{15} (m_o/m^*)^{\frac{1}{2}} \epsilon_s^2 T^{3/2}}{(2N_A + n_o)\{\ln(b+1) - [b/(b+1)]\}} \text{ cm}^2/\text{V.see} \quad (3)$$

$$\text{where } b = \frac{1.29 \times 10^{14} (m^*/m_o) \epsilon_s T^2}{n^*} \quad (4)$$

where n^*, the effective screening density is given by

$$n^* = n + [(n_o + N_A)(N_D - N_A - n_o)/N_D] \text{ cm}^{-2} \quad (5)$$

where N_D and N_A are respectively the density of donars & acceptors and for the temperature of interest (< 150 K), $n_o \simeq N_D - N_A$.

The interaction of the electrons with the perturbing potential produced by the lattice vibrations may be described only by adopting a quantummechanical description of the vibrations. The lattice vibrations, or phonons, interact with electrons obeying the principles of conservation of energy and momentum. For (Al,Ga)As the dispersion

relation has two groups of branches. The in-phase vibration called acoustic phonons give rise to potential discontinuities which accounts for deformation potential scattering. This has been derived by Bardeen and Shockley [34] as

$$\mu_{dp} = \frac{2\,(2\pi)^{\frac{1}{2}}\, q\hbar^4\, \rho\, w_\ell^{\,2}}{3\,(m^*)^{5/2}\,(k_o T)^{3/2}\, E_1^{\,2}} \tag{6}$$

$$= \frac{(3.2 \times 10^{-5})\, \rho\, w_\ell\; T^{-3/2}}{(m^*/m_o)^{5/2}\, E_1^{\,2}} \tag{7}$$

where ρ and w_ℓ are the mass density and the longitudinal sound velocity respectively. E_1 is the deformation potential in electron volts.

The atoms constituting the crystal being partially ionised, the displacements of the atoms due to acoustic vibrations produces

the piezoelectric potential. Since GaAs or (Al,Ga)As lacks inversion symmetry the scattering of electrons through the piezo electric potential becomes important above 77K.

The relexation time for piezoelectric scattering as determined by Zook [35] is given by

$$\frac{1}{\tau_{PE}} = 1.05 \times 10^7 . e_{14}^{\,2} \left(\frac{4}{c_t} + \frac{3}{c_\ell}\right) \left(\frac{m^*}{m_o}\right)^{\frac{1}{2}} T^{\frac{1}{2}}\, \chi^{-\frac{1}{2}} \tag{8}$$

where χ is the electron energy in kT

where e_{14} is the one independent piezoelectric constant in V/cm and the average longitudinal and transverse elastic constants are

$$c_\ell = \frac{1}{5}\,(3C_{11} + 2\,C_{12} + 4C_{44})$$

$$c_t = \frac{1}{5}\,(C_{11} - C_{12} + 3C_{44}) \quad \text{in dynes /cm}^2 \tag{9}$$

$$\langle\tau\rangle = \frac{4}{3\pi^{\frac{1}{2}}} \int_0^\infty \tau(\chi)\, \chi^{3/2} \exp(-\chi)\, d\chi \tag{10}$$

$$\mu = \frac{e\langle\tau\rangle}{m^*} \tag{11}$$

In the second group of vibrations of the lattice the neighbouring atoms vibrate in opposite phase. The vibrations give rise to optical phonons which also produce perturbing potentials in two ways. The deformation of the crystal due to optical vibrations produce a perturbing potential proportional to the optical strain. The interaction of the electrons with the lattice through the deformation produced by optical vibrations is very much dependent on the symmetry of the band structure. This interaction is very weak for electrons at the Γ-point minima or for the X-point minima. Since for most of the values of Al -content the electrons reside either in the Γ or X valley the non-polar optic phonon scattering is not considered in the analysis.

The polar optical phonon scattering occurs through the polarisation produced by the optical vibrations due to ionic charges. This is particularily important at higher temperatures. The energy of the optical phonons is usually comparable to that of the electrons at ordinary temperatures since the equivalent temperature of the optical phonons (θ) of almost all semiconductors lies between 150K and 500K. The energy of phonons cannot therefore be neglected in comparison to that of electrons and the collision should be considered as inelastic. Following the analysis of Fortini [36] the mobility limited by polar

optical phonon scattering is given by

$$\mu_{PO} = \frac{16\,\hbar\,\epsilon_s\,(2\,\pi\,k_o T)^{\frac{1}{2}}\,(e^{\theta/T}-1)}{3q\,\omega_l\,(m^*)^{3/2}\,(\frac{1}{\epsilon_d}-\frac{1}{\epsilon_s})}\,G\,(\frac{\theta}{T}) \quad (12)$$

$$= 25.44\,\frac{\epsilon_s\,.\,\epsilon_d}{\epsilon_s-\epsilon_d}\cdot\frac{Exp\,(\theta/T)\,-1}{(m^*/m_o)^{3/2}\,\theta}\cdot G\,(\frac{\theta}{T})\cdot T^{\frac{1}{2}} \quad (13)$$

where $G(\frac{\theta}{T})$ is the fortini's function given by

$$G(\frac{\theta}{T}) = \int_o^{\infty} \mathcal{V}(\xi,\theta).\, d\xi \quad (14)$$

$$\omega_l = \frac{k_o\theta}{\hbar} \quad (15)$$

Finally, in a real crystal there is a host of electrons which are relatively free. The concentration of these free electrons range typically between 10^{13} and 10^{18} cm^{-3}. Hence, even when we confine our attention to a single electron and assume that the states obtained from this one-electron approximation represent the available states for the free electrons, we should take into consideration the fact that the state of the electron may be changed by collision with another free electron when they come near each other through their Coulomb fields. Such collisions are called carrier-carrier or space charge scattering. From Weisberg's [37] analysis the space charge scattering limited mobility is given by

$$\mu_s = q\,[N_s\,(2\,m^*\,k_o T)^{\frac{1}{2}}\,A]^{-1} \quad (16)$$

$$= \frac{(3.2 \times 10^9)\,T^{-\frac{1}{2}}}{(m^*/m_o)^{\frac{1}{2}}\,(N_s A)} \quad (17)$$

where N_s is the concentration of space charge and A is the effective scattering area of the space charge region.

Equations (1-17) was sufficient to explain the temperature variation of mobility for Si-implanted GaAs.

An additional scattering mechanism is present in mixed crystals such as $Al_xGa_{1-x}As$ due to the random distribution of the component atoms among the available lattice sites. An expression for mobility limited by alloy scattering was first derived by Brooks (unpublished work) and later developed by Hauser et al [38-40, 42, 59], Chandra and Eastman [43], and Saxena and Gurumurthy [44] for $Al_xGa_{1-x}As$ to be

$$\mu_A = \frac{52.83\ T^{-\frac{1}{2}}}{(m^*/m_o)^{5/2}\ x(1-x)(\Delta U)^2} \tag{18}$$

where ΔU is the alloying alloy scattering potential.

For $x \geqslant 0.3$ in $Al_xGa_{1-x}As$ the intervalley separations become small and considerable electron transfer to the X or L valleys can take place even at temperatures as low as 77K. Since electrons in the L and X valleys have lower mobilities compared to those in the Γ valley, the effect of the transfer is to lower the measured average mobility. At very high values of Al-content the L & Γ valleys are so much higher in energy than the X valley that the mobility is essentially determined by the properties of the X valleys.

Thus at the intermediate range of a values there might be electrons scattered among the three X minima or the four L minima. In addition there might be scattering of electrons between the L and X minima. Each scattering process involves the absorption or emission of phonons.

In general the scattering rate from a state k in the valley "i" to a state k' in valley "j" has been derived by Fawcett et al [45]. Using this expression and approximation $E = (\frac{3}{2})\, k_o T$, the mobility limited by non-equivalent intervalley scattering can be expressed as

$$\mu_{IV} = \frac{8\sqrt{\pi}}{3(m_j^*)^{5/2}} \cdot \frac{q\, \hbar^2 \rho \sqrt{k_o \theta}}{\sqrt{3}\; N_j\, D_{ij}^2} \left[\frac{\left(\frac{T}{\theta} + \frac{2}{3} + \frac{\Delta E_{ij}}{k_o T}\right)^{\frac{1}{2}}}{(e^{\theta/T} - 1)} + \frac{\left(\frac{T}{\theta} - \left(\frac{2}{3} + \frac{\Delta E_{ij}}{k_o T}\right)\right)^{\frac{1}{2}}}{(1 - e^{-\theta/T})} \right]^{-1}$$

$$\text{for } \frac{T}{\theta} \geqslant \frac{2}{3} + \frac{\Delta E_{ij}}{k_o T} \qquad (19)$$

The last term on the right hand side is zero for $\frac{T}{\theta} < \frac{2}{3} + \frac{\Delta E_{ij}}{k_o T}$

N_j is the number of equivalent minima and m_j^* is the mass in a single minimum. ΔE_{ij} is the intervalley separation. $(N_j^{2/3}\, m_j^*)$ is the combined density-of-states mass for the valley "j". D_{ij} is the coupling coefficient for the proper valleys.

For equivalent intervalley scattering the above expression is applicable when N_j is changed to $(N_j - 1)$ and $\Delta E_{ij} = 0$. The values of coupling coefficients D_{XX} and D_{LX} have been taken from Saxena and Gurumurthy [44] and these values agree reasonably well with earlier published data [46]. The value of θ is taken from Birman et al [47],

$$\theta = \theta_{LO}^{x}$$

The optical phonon temperature (θ) was calculated for the previous mobilities by selecting the proper values of the electron wavelength for a particular value of x for each GaAs and AlAs from Fig 2.3 [48]. Then relation $E = h\nu$ was used to calculate E and find θ from

$$\theta = \frac{E}{k_o} \qquad (20)$$

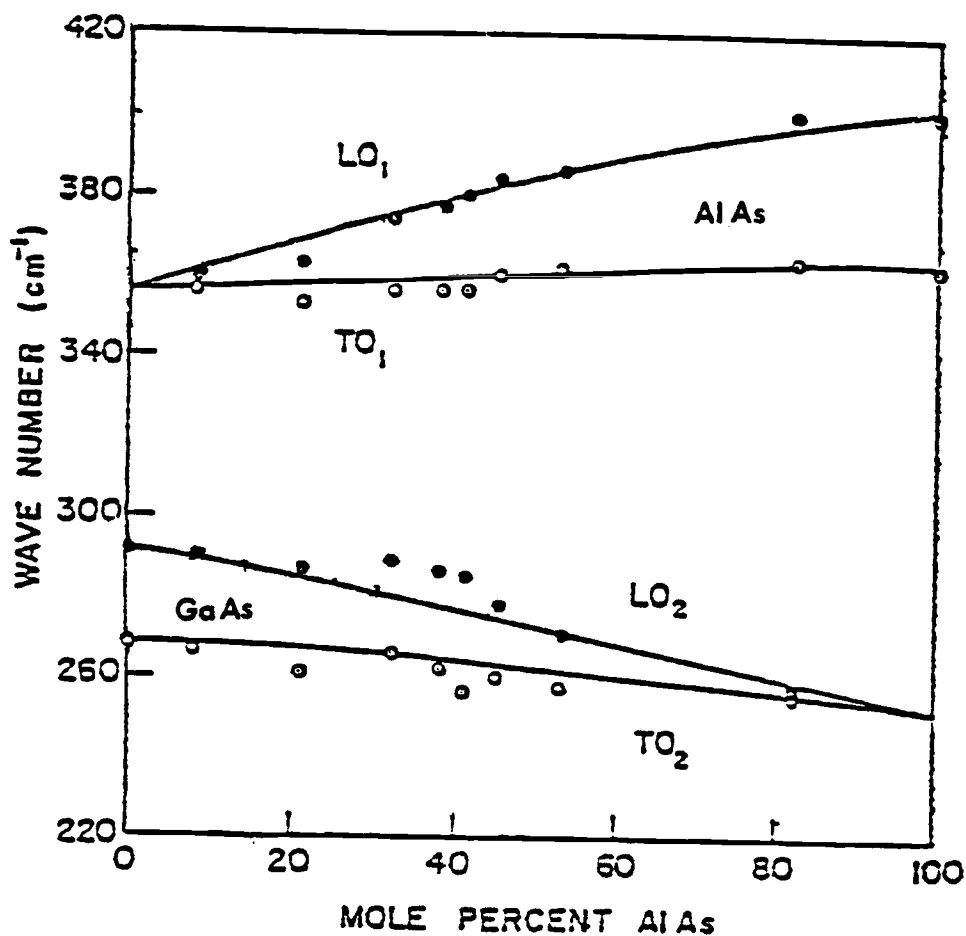

Fig. 2.3 TO and LO mode frequencies, as obtained from a Kramers-Kronig analysis of the mixed crystal spectra, plotted versus alloy composition. The solid lines are calculated from the REI model (Ref. p. 378 [48])

The actual Θ was found out from the relation

$$\Theta_{LO}(x) = x\ \Theta_{AlAs} + (1 - x)\ \Theta_{GaAs} \tag{21}$$

In this study we have taken $E_1^{\Gamma} = 8.6$ e.V. as constant and E_1^{x} from 300K data [44] Fig 2. The value of E_1^{L} is unknown. The variation of the effective mass of electrons in the Γ valley is obtained from $\vec{k}.\vec{p}$ theory [49] as

$$\left(\frac{m_o}{m^*_{\Gamma}}\right) = 1 + 7.51\left(\frac{2}{E_{\Gamma}} + \frac{1}{E_{\Gamma} + 0.341}\right) \tag{22}$$

Since the energy of the X-minima remains almost invariant with x, a constant value of the density-of-states effective mass $m^*_X = 0.35m_o$ in a single minimum has been used [50]. Using $\vec{k}.\vec{p}$ theory to calculate the transverse effective mass m_t in the L minima and knowing that the longitudinal effective mass $m_{\ell} = 1.9\ m_o$, it has been found [23] that

$$m^*_L = N^{2/3}\ m_t^{2/3}\ m_{\ell}^{1/3} \simeq (0.55 + 0.076\ x)\ m_o \tag{23}$$

where N = 4 for L minima.

The parameters $\epsilon_s, \epsilon_d, \rho, c_t, c_{\ell}$ and w_{ℓ} were determined by a linear interpolation of the values for GaAs [51, 52] and AlAs [53, 54]

$$\text{i.e. } \alpha_{Al_xGa_{1-x}As} = x\ \alpha_{AlAs} + (1-x)\ \alpha_{GaAs} \tag{24}$$

Assuming the validity of Boltzman statistics in multivalley conduction the following relations can be written:

$$n_\Gamma = N_c^\Gamma \text{ Exp } (E_F/k_oT) \tag{25a}$$

where $$N_c^\Gamma = \frac{4\sqrt{2}}{h^3} (\pi m^*_\Gamma k_oT)^{3/2} \tag{25b}$$

and $$\frac{n_L}{n_\Gamma} = (\frac{m^*_L}{m^*_\Gamma})^{3/2} \text{ Exp } (-\frac{\Delta E_{\Gamma L}}{k_oT}) \tag{26}$$

$$\frac{n_X}{n_\Gamma} = (\frac{m^*_X}{m^*_\Gamma})^{3/2} \text{ Exp } (-\frac{\Delta E_{\Gamma X}}{k_oT}) \tag{27}$$

E_F is the fermi energy

where $\Delta E_{\Gamma L}$ and $\Delta E_{\Gamma X}$ are the Γ-L and Γ-X intervalley seperations, respectively. The effective mobility can be expressed as

$$\mu_H = \frac{\mu_\Gamma [1 + \frac{n_X}{n_\Gamma} (\frac{\mu_X}{\mu_\Gamma})^2 + \frac{n_L}{n_\Gamma} (\frac{\mu_L}{\mu_\Gamma})^2]}{1 + \frac{n_X}{n_\Gamma} \cdot \frac{\mu_X}{\mu_\Gamma} + \frac{n_L}{n_\Gamma} \cdot \frac{\mu_L}{\mu_\Gamma}} \tag{28}$$

Since most of the parameters for the L minima are unknown it is assumed that $\mu_\Gamma/\mu_L \approx 7.5$ as in GaSb determined by Sager and Kisicki [56, 57].

An empirical formula for N_sA was derived by Kaneko [49] and Stringfellow [59] as

$$N_sA = 5 \times 10^3 + 6.3 \times 10^5 \quad (cm^{-1}) \tag{29}$$

The value of the alloy scattering potential, ΔU, is given by Saxena [28] as

$$\Delta U = 0.3 + 0.0011 x \tag{30}$$

These values were used as the starting trial values but were adjusted to best fit the data.

Since only n-type samples of $Al_xGa_{1-x}As$ were measured, the temperature dependence of n_H was analysed based on a model with three conduction bands Γ , L and X, two donor levels, and one acceptor level. The total number of carriers in the three conduction valleys and like impurity levels must satisfy the charge neutrality condition:

$$\text{i.e.} \quad N_{D1} + N_{D2} - N_A = n_1 + n_2 + n_\Gamma + n_L + n_X \qquad (31)$$

where $n_{D1,2}$ are the density of donors, $n_{1,2}$ are the density of occupied donors at levels $E_{D1,2}$ and N_A is the density of acceptors.

$n_{\Gamma,\ L,\ X}$ are the density of electrons in the Γ, X, L minima. The concentration of carriers were found from eqns. [25-27]. The density of electrons in the donor states were found from the equation.

$$n_{1,2} = \frac{N_{D1,2}}{1 + \frac{1}{2}\ \mathrm{Exp}\ [(E_{D1,2} - E_F)/k_oT]} \qquad (32)$$

Then the hall concentration of carriers was found out from

$$n_H = \frac{n_\Gamma \left(1 + \frac{n_x}{n_\Gamma} \cdot \frac{\mu_x}{\mu_\Gamma} + \frac{n_L}{n_\Gamma} \cdot \frac{\mu_L}{\mu_\Gamma}\right)}{\left[1 + \frac{n_x}{n_\Gamma}\left(\frac{\mu_x}{\mu_\Gamma}\right)^2 + \frac{n_L}{n_\Gamma}\left(\frac{\mu_L}{\mu_\Gamma}\right)^2\right]} \qquad (33)$$

2.2 High-Field Transport:

When a high-field is applied to a semiconductor the electrons in it are heated to a temperature higher than that of the lattice and occupies higher energy levels in the Γ conduction minima. When the electron energy is high enough, some of them may be transferred to the

sattelite valleys, in which the electrons have a low mobility. Accounting for the density and mobility of carriers in all conduction minima the ratio of the hall to drift mobility of electrons, μ_H/μ_d, assuming unity hall scattering factors in all conduction minima, is given by

$$\frac{\mu_H}{\mu_d} = \frac{n_T}{n_H} = \frac{(1 + \frac{n_L}{n_\Gamma} + \frac{n_x}{n_\Gamma})\ [1 + \frac{n_L}{n_\Gamma} (\frac{\mu_L}{\mu_\Gamma})^2 + \frac{n_x}{n_\Gamma} (\frac{\mu_x}{\mu_\Gamma})^2]}{(1 + \frac{n_L}{n_\Gamma} \cdot \frac{\mu_L}{\mu_\Gamma} + \frac{n_x}{n_\Gamma} \cdot \frac{\mu_x}{\mu_\Gamma})} \tag{34}$$

where $n_T = n_\Gamma + n_L + n_X$

and $$\frac{n_{L,x}}{n_\Gamma} = (\frac{m^*_{L,X}}{m_\Gamma})^{3/2}\ \text{Exp}\ (-\frac{\Delta E_{\Gamma X,\Gamma L}}{k_o T}) \tag{35}$$

where $(n, m^*, \mu)_{\Gamma, L, X}$ are the respective transport parameters in the three sets of minima, and $\Delta E_{\Gamma X,\Gamma L}$ are the energy separations of the X and L minima from the Γ minimum.

2.3 Principle of the Probe Technique of v-$\mathcal{E}$ Measurements

By knowing the potential distribution V(x) along the bridge of the H-device Fig [2.5(a)] for a device current I, the electric field distribution $\mathcal{E}(x)$ may be determined. The current density J(x) flowing through the device is I/A where A is the cross-sectional area of the region (taken to be uniform) where the field is measured. A relationship is thus obtained which expresses the current density J as a function of the electric field $\mathcal{E}$. Near the origin this characteristic will be linear, since here the device will be in the ohmic region. It follows that for this region $J = \sigma\mathcal{E}$. The slope of the J-$\mathcal{E}$

characteristic near the origin will therefore give the value of σ which may be compared with the value obtained from the Van der Pauw measurement. Also in the ohmic region, $v = \mu_d \mathcal{E}$. Thus the J-$\mathcal{E}$ curve may be transformed to a velocity-field characteristic. The potential distribution along the H-device is measured by a high impedance probe.

In order to gain further understanding of the principle of the measurement consider a $v(\mathcal{E})$ curve that is linear up to a threshold field $\mathcal{E}_T$ and saturates at a velocity v_s (Fig 2.4). It is assumed that the carrier concentration remains constant at all bias fields, and that the electric field changes abruptly when a new cross-section is encountered. Refering to Fig 2.5 the following may be written:

$$V_1 = E\ell_1 \quad ; \quad I_1 = n_o q v A_1$$
$$V_2 = E\ell_2 \quad ; \quad I_2 = n_o q v A_2 \qquad (36)$$

Where V_1 & I_1 apply to the contact area, and V_2, I_2 apply to the bridge. A_1 and A_2 are the cross-sectional area in contact area and bridge, respectively. Since the currents through the whole device must be constant, adding the voltages for the two sections will give the I-V relation for the complete device, (Fig 2.6).

Since the saturation current is $n_o q v_s A_2$ and the voltage across the contact region remains constant at $R_1 I_{sat}$ when saturation sets in, any increase in device voltage will be developed across the bridge, thus increasing the electric field therein. At the threshold point the electric field in the contact region would be

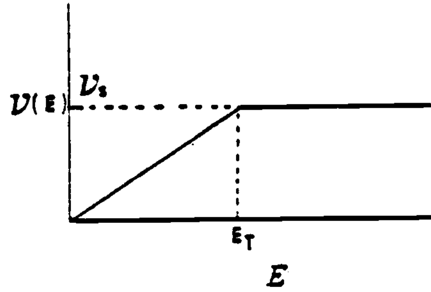

Fig 2.4 A simplified picture of the velocity field characteristic in the bridge of the H-Device.

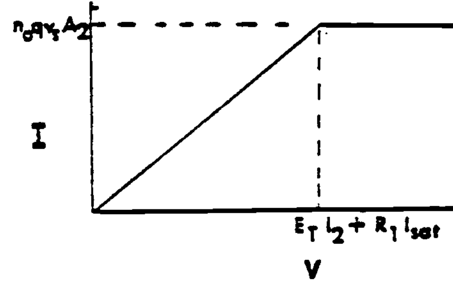

Fig 2.6 A simplified picture of the current-voltage characteristic of a complete H-device.

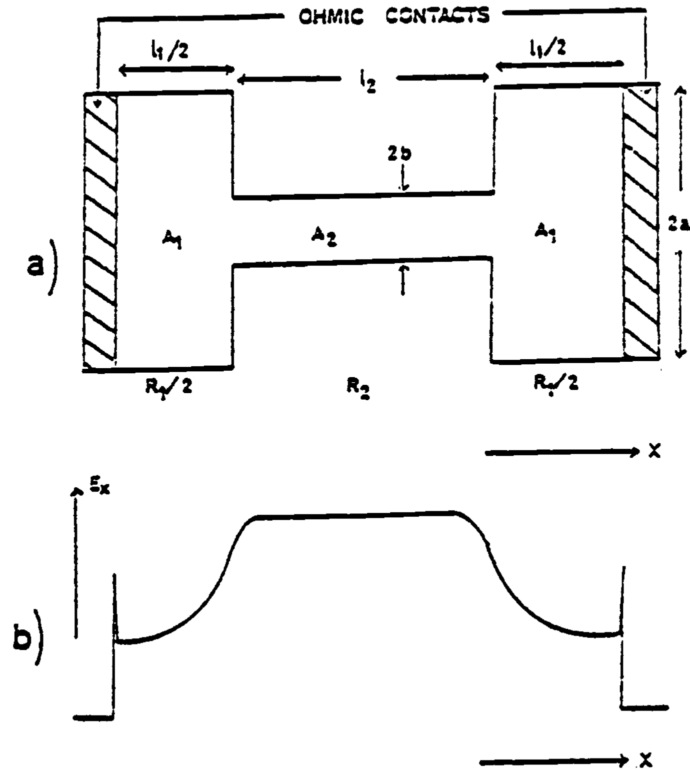

Fig 2-5 Top (a) H-device geometry

Bottom (b) Expected field distribution

$$\mathcal{E}_1 = \frac{1}{\sigma} \cdot \frac{l_1}{A_1} \cdot \frac{n_o q \, \vartheta_s \, A_2}{l_1} \tag{37}$$

where $\vartheta_s = \mu_D \mathcal{E}_T$ and $\frac{1}{\sigma} = \frac{1}{n_o q \; \mu_D}$ (38)

where μ_D is the low field drift mobility of the material. From these we get

$$\frac{\mathcal{E}_1}{\mathcal{E}_T} = \frac{A_2}{A_1} \tag{39}$$

It is known that the low-field part of the $\vartheta(\mathcal{E})$ curve departs from linearity at fields higher than $\sim \mathcal{E}_T/2$. Thus to keep the contact region in the linear portion of the $\vartheta(\mathcal{E})$ curve the field should be restricted to a value $\mathcal{E}_1 \leqslant \mathcal{E}_T/2$. One other condition that has to be satisfied is: $\mathcal{E}_1 < \mathcal{E}_{sust.}$ where $\mathcal{E}_{sust.}$ is the sustaining field for a domain. From earlier work it is known that $\mathcal{E}_{sust.} \lessapprox \mathcal{E}_T/1.7$, or $A_1 \geqslant 2A_2$. Thus for a device of constant layer thickness the condition $a \geqslant 2b$ should be satisfied. The electric field cannot change abruptly when a new cross-section is encountered. For the electric field to become approximetely uniform and have only an x-component at the metal contact and in the bridge, the following must hold:

$$\frac{l_1}{2} \geqslant a \tag{40}$$

$$\text{and } l_2 \geqslant b \tag{41}$$

These are the main design criteria used for the fabrication of the H-devices.

Chapter 3

Experimental Techniques

3.1 Material Description

Undoped and Si-doped $Al_xGa_{1-x}As$ layers 5-10 μm thick and with $0 < x \leq 0.6$ grown on (100) GaAs: Cr substrates at 750°C with a V/III ratio of $\sim$10 were used for the $Al_xGa_{1-x}As$ measurements. Some of the layers studied were grown at 690°C with a V/III ratio of 25. The alloy compositions were determined from the peak energy of photoluminescence at 1.9 or 4.4K.

The implanted GaAs samples used in this study were of device quality suitable for the fabrication of field-effect transistors. They were made by implanting 140 keV Si-ions in doses ranging from 8×10^{11} to 5×10^{12} cm^{-2} into 200 μm thick undoped LEC GaAs wafers. Post implantation annealing of the samples covered by a proximity cap was done at 800°C for 30 mins in a H_2 atmosphere.

3.2 Hall Measurements

The measurement of low field mobility was done by the Van der Pauw's method [68]. A flow chart of the preperation and measurement of samples is shown in Fig 3.1. Square Hall measurement samples with 0.5 cm sides were scribed from the wafers. The samples were cleaned in organic solvents and etched in HCl before contact metal deposition. The metals used were Ag-Sn for $Al_xGa_{1-x}As$ and Au-Ge/Ni for GaAs. Details of the metallization process are described in Table 3.1.

Schematics of the sample mounting assembly is shown in Fig 3.2. A magnetic field of 0.4 or 0.5 Tesla was used. Voltages were measured

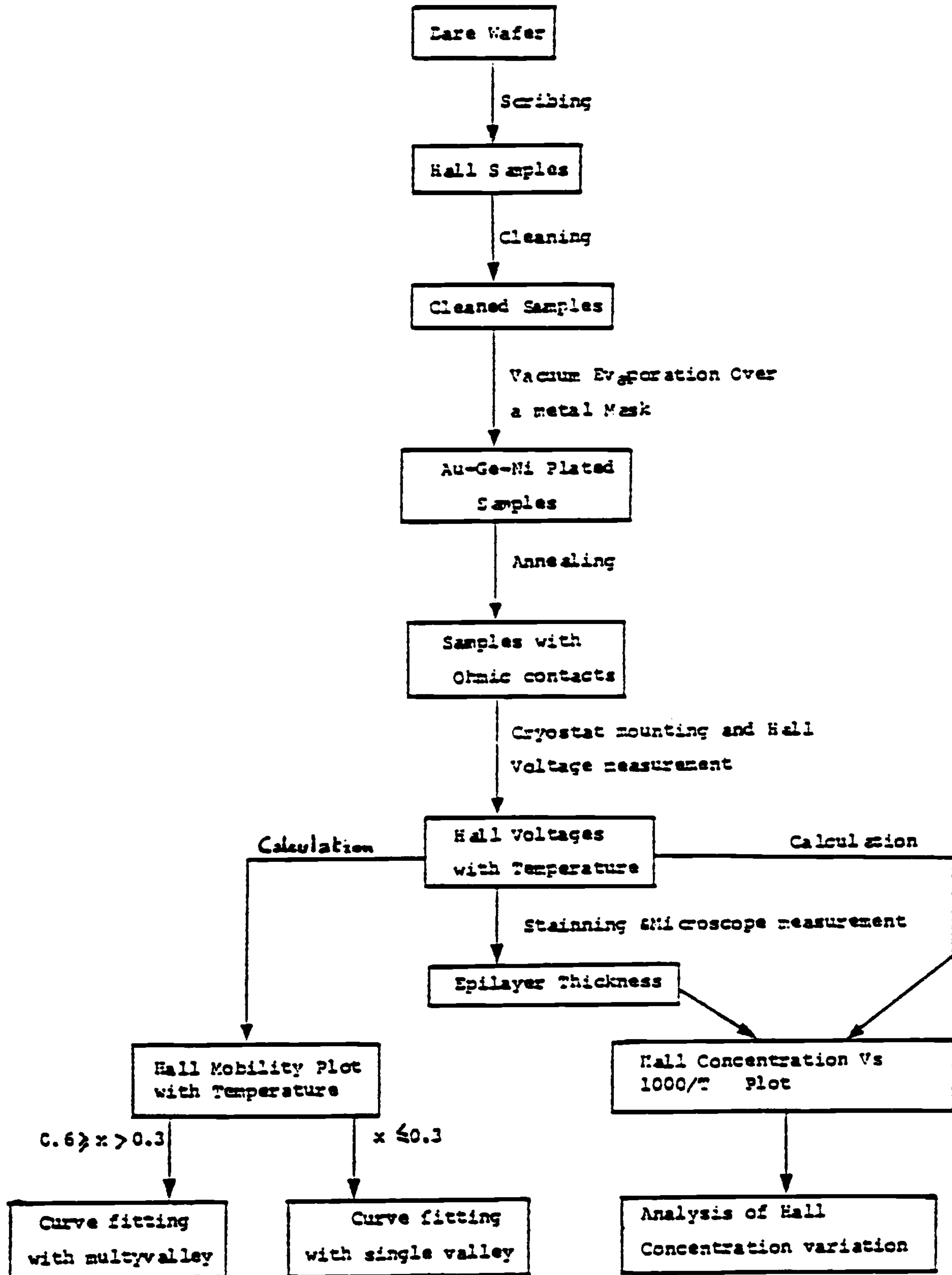

Fig 3.1 Flow chart for preperations of Hall Samples and Hall measurement.

TABLE 3-1

Summary of the metallization and alloying process for the fabrication of ohmic contacts.

Vacuum Pressure	Metal	Weight of Metal	Distance of Substrate from source	Source Heater	Alloying Temperature	Alloying Time	N_2 Flow rate
	Ag-Sn	250mg			$350^{\circ}C$		
10^{-6}--10^{-7} Torr.			10 cm.	Ta or Mo boat		1-2 min.	5litres per minute
	(Au,12%Ge)-Ni	100mg --5mg			$400^{\circ}C$		

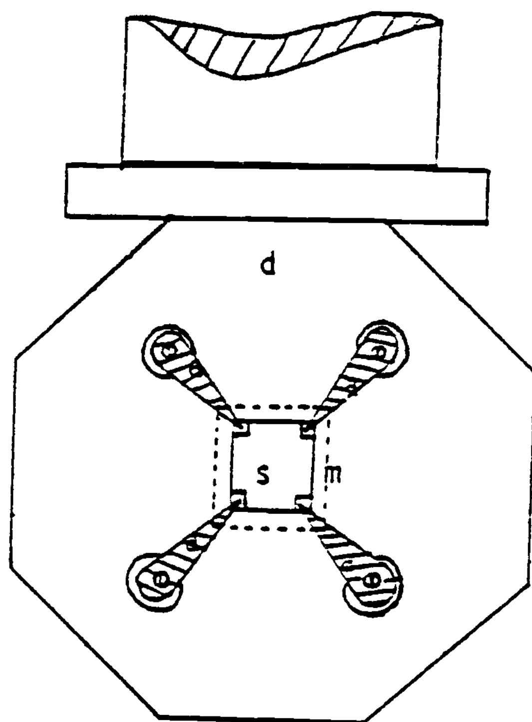

Fig 3-2 : Mounting of the sample on the cryostat.
a) Phosphor-bronze spring contact probes d) Cryostat holder m) Mica sheet insulator s) Sample with ohmic contacts.
Magnetic field is perpendicular to the plane of the diagram.

with an accuracy of 0.01 mV and the currents with an accuracy of 1 μA. Constant currents of the order of 100 μA were normally used. The contacts on some samples were ohmic at room temperature but showed non-ohmic behavior at low temperatures. Although the effects of contact resistance are largely eliminated by taking measurements at reversed polarities of the magnetic field and current, the samples with non-ohmic contacts at low temperatures were not used.

3.3 High-Field Measurements

The flow chart for the preperation of H-devices and the measurement of high-field mobility is depicted in Fig 3.3 The devices were fabricated photolighographically with the use of a positive photoresist and mesa etching with 1 H_2SO_4: 1 H_2O_2: 1 H_2O. A schematic diagram of the measurement system is given in Fig 3.4. It was found that a Ni-probe was better suited for $Al_xGa_{1-x}As$ and a W-probe scratched the samples. A probe tip of 10 μm or less was obtained by chemical etching with a solution of 25 gm Fe_3Cl in 100 ml of H_2O. The potential and current-voltage measurement were done with a pulsed voltage (40 n.s., 100-200 Hz) to avoid resistive heating of the device. The attenuator was calibrated at lower voltages and this calibration was assumed to be constant at higher voltages. The least count for the verniers attached to the probe was 10 μm. The device resistance increased with the Al-content in the sample from a few hundred ohms to a few kilo ohms. With reference to Fig 2.5(a) the best results were obtained with the following two device dimensions:

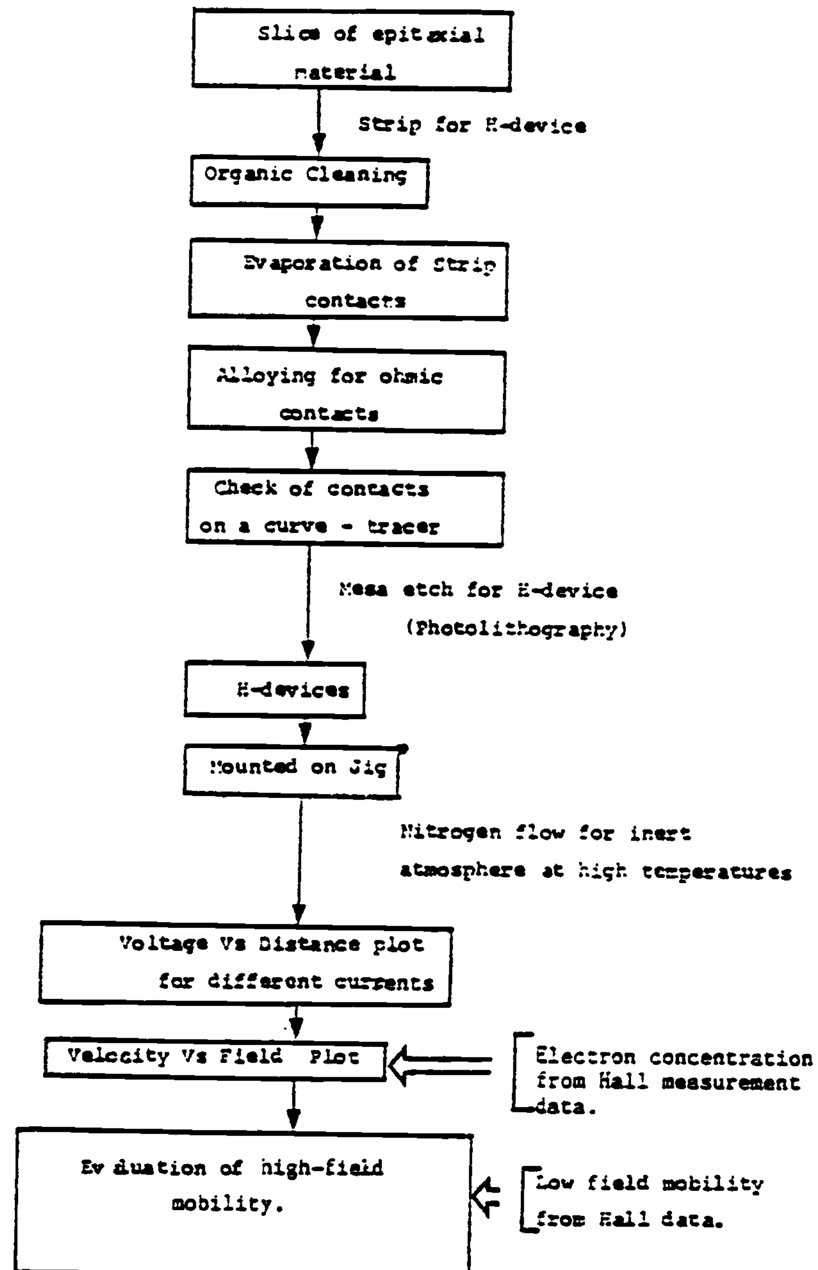

Fig 3.3 Flow chart for the preperation of H-devices and measurement of high-field mobility.

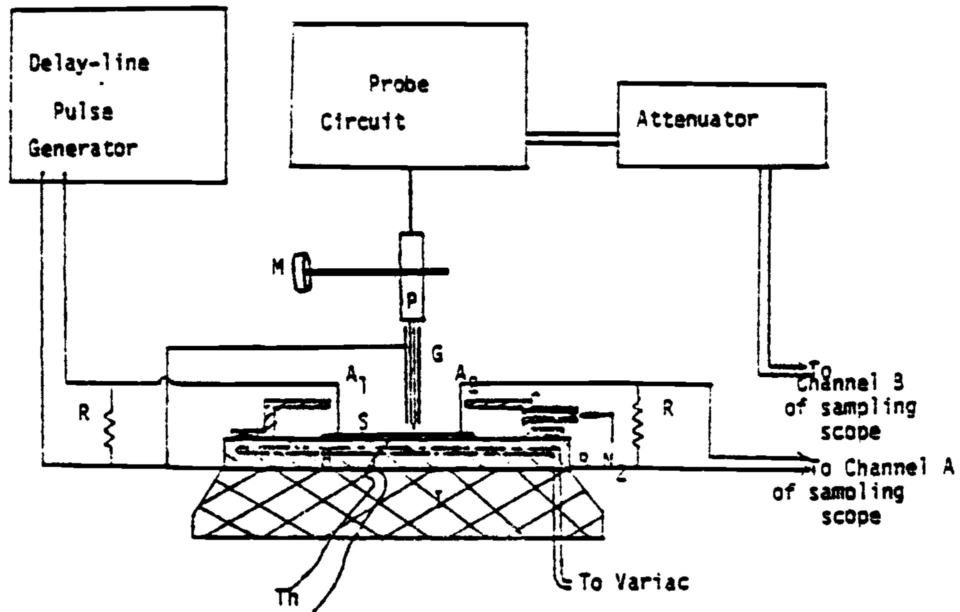

M: Micrometer Screw
P: 100 K Probe
A_1 , A_2 : Ohmic Contacts to the end pads
S : H-Device Sample
H : Heater
Th : thermocouple
C : Brass cover with inlet for Nitrogen gas
B : Stainless Steel jig to hold the sample
I : Insulated base
G : Grounded Shield
R : Terminating Resistance

Fig 3.4 Measurement setup for high-field mobility.

(i)
$\frac{\ell_1}{2} = 700\ \mu m$
$\ell_2 = 600\ \mu m$
$a = 400\ \mu m$
$b = 150\ \mu m$
$c = 1500\ \mu m$

(ii)
$\frac{\ell_1}{2} = 700\ \mu m$
$\ell_2 = 750\ \mu m$
$a = 400\ \mu m$
$b = 150\ \mu m$
$c = 1500\ \mu m$

A heating element inserted in the sample jig and fed by a variable power supply was used for high-temperature measurements. Low temperature measurements were tried by cooling the jig with N_2 gas circulated through a liquid nitrogen bath, but water vapour condensation on the sample made it impossible to get any reliable data.

The current through the device was calculated from the terminating resistance value and the voltage measured across it. Since the carrier concentration (n) is known from the Hall measurements, the electron velocities can be calculated from:

$$\vartheta = \frac{I}{nqA} \tag{42}$$

where I is the current, q the electronic charge and A the cross-section which was taken to be equal to A_2. The field was calculated from the slope of the potential distribution curve.

Chapter 4

Transport and Associated Effects in Ion-Implanted GaAs

Plots of the measured and calculated mobilities are given in Figs 4.1 and 4.2 for the Si-implanted GaAs samples. The program used for the analysis of mobility data is given in Appendix I and the various parameters used for the analysis is given in Table 4.1. A summary of the analyzed results is presented in Table 4.2. From the mobility analysis it is clear that the compensation for these samples is very large. For most of the samples it is found that it is very difficult to fit the low-temperature part of the data with the existing theory. This is in compliance with the unusual increase of the Hall carrier concentration at very low temperatures depicted in Fig 4.3. The same effect was also observed in some $Al_xGa_{1-x}As$ samples and therefore it may be inferred that the substrate or the substrate-active layer interface contribute to it.

As shown in Fig 4.4, at low temperatures the ionised impurity scattering is predominant but at high temperatures optical phonon and space-charge scattering become relatively important.

Comparing the volume concentration of carriers, obtained from the mobility analysis with the concentration per unit area evaluated from the Hall measurement, the implantation depth was found to be around 1μm approximately.

On the other hand considering the measured value of sheet carrier concentrations for E514 and E522 with the volume concentration obtained from the mobility analysis the implantation depth is much less than 1μm.

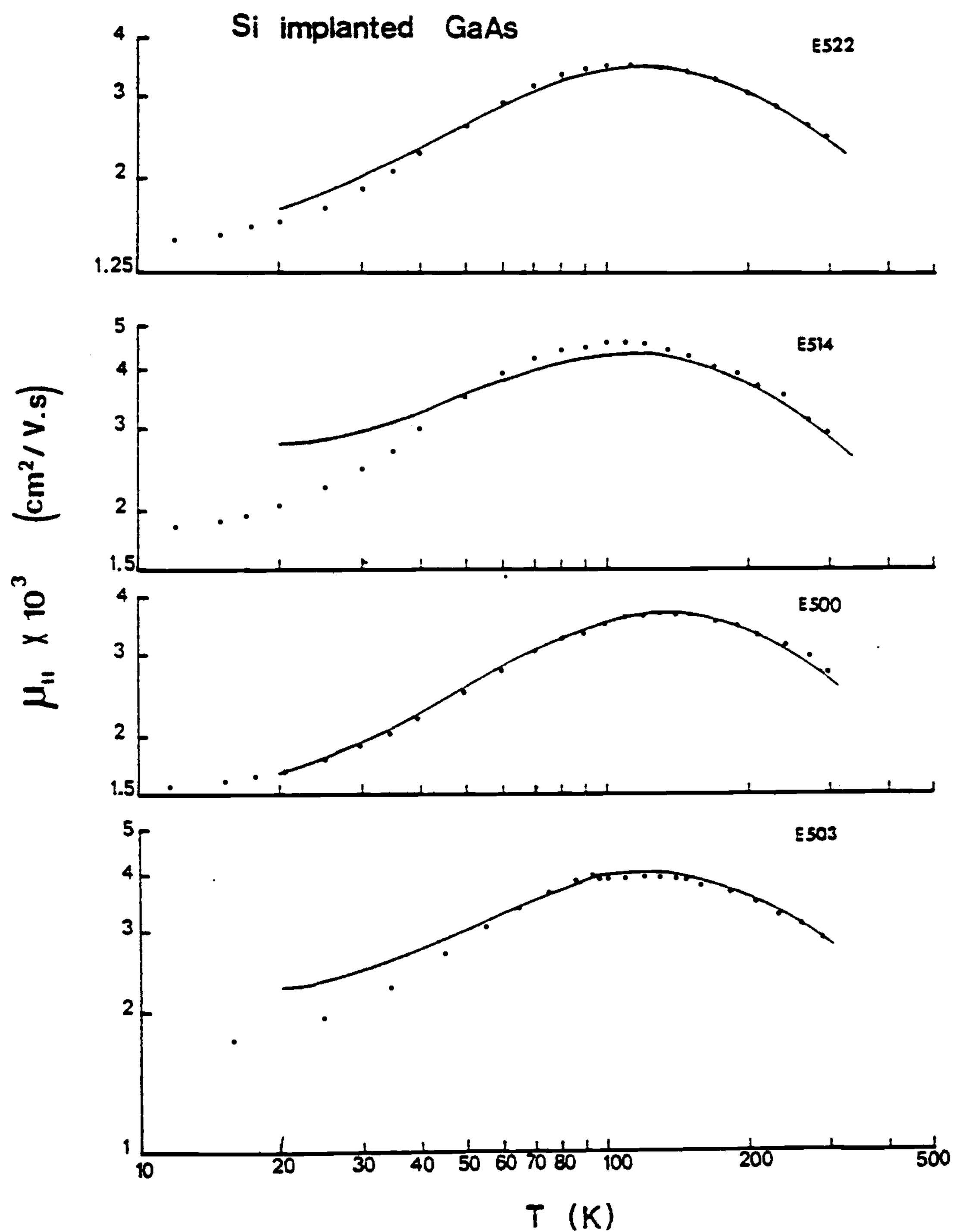

Fig 4.1 Measured variation of the Hall mobility with temperature for Si-implanted GaAs samples.

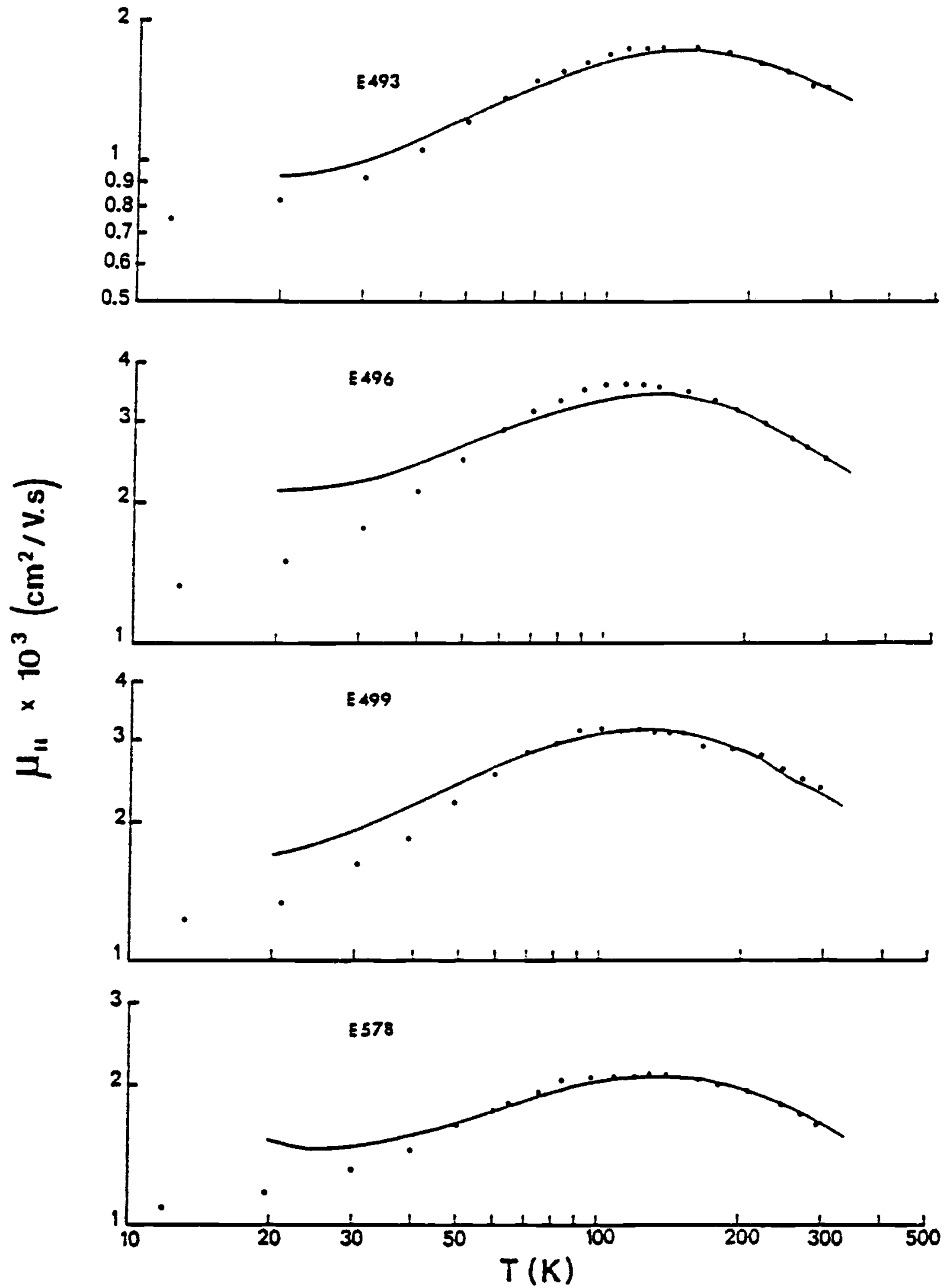

Fig 4.2 Measured varriation of the Hall mobility with temperature for Si-implanted GaAs samples.

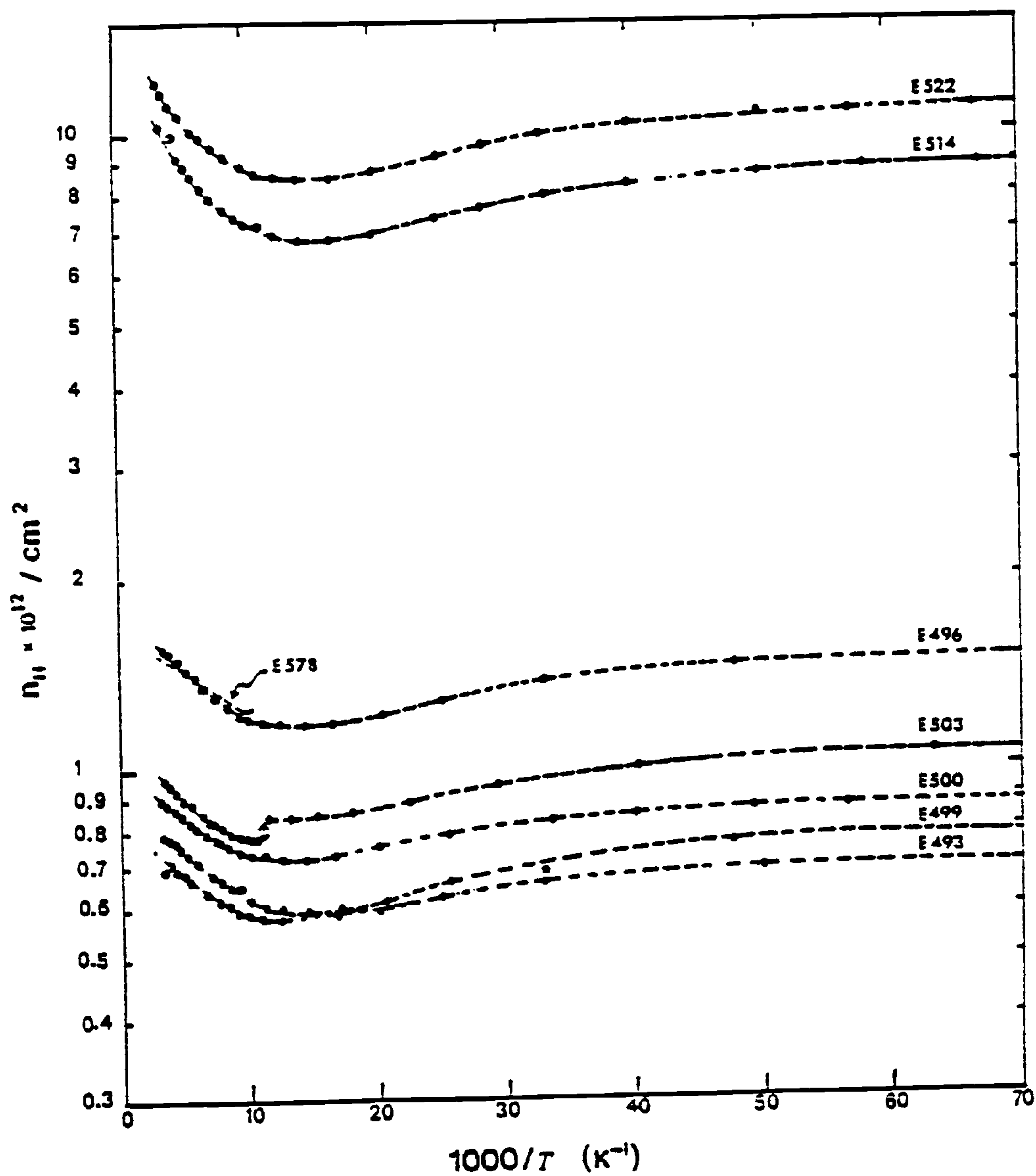

Fig 4.3 Measured variation of the sheet carrier concentration with temperature for the Si-implanted GaAs samples, from Hall measurement.

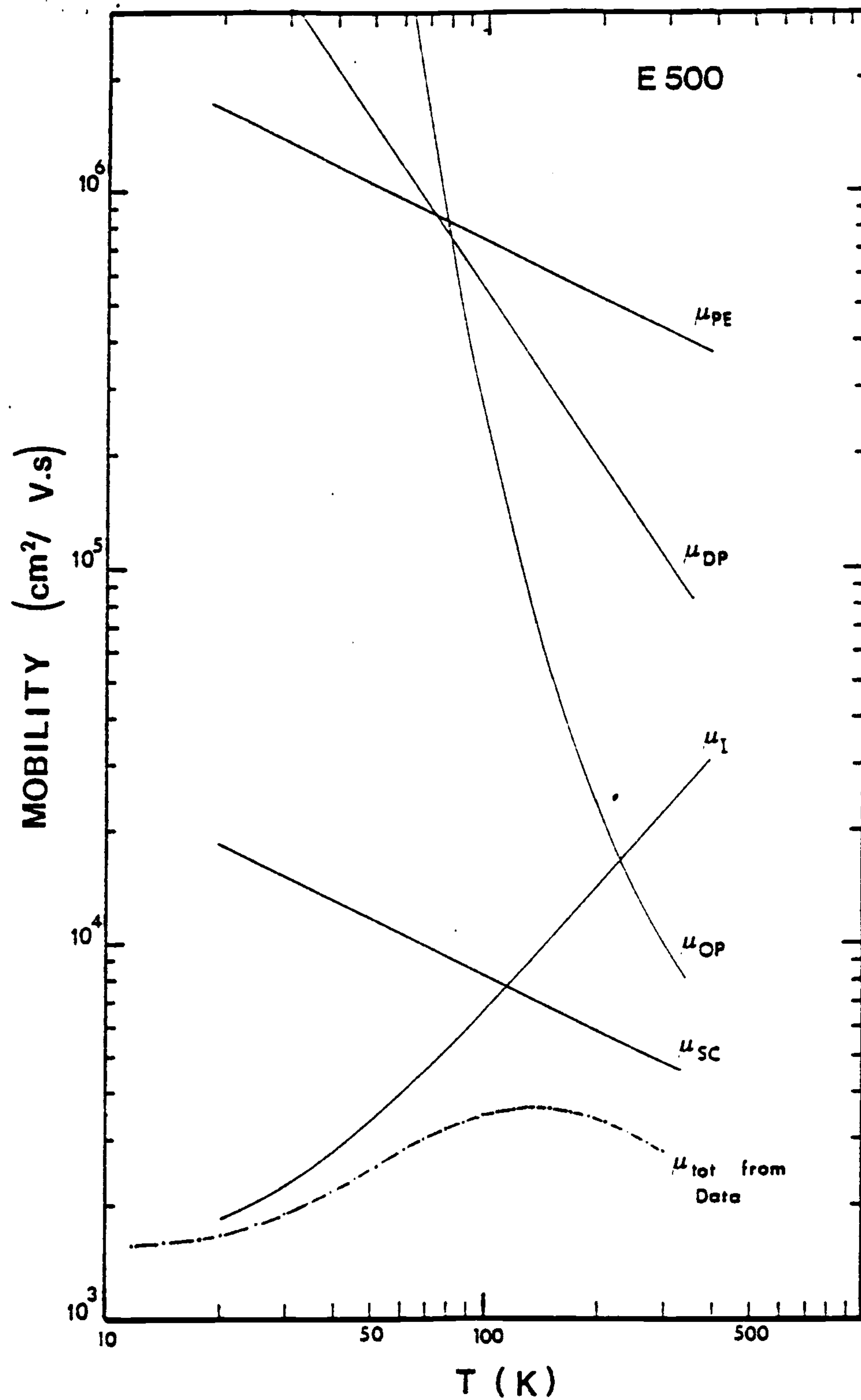

Fig 4.4 Values of the mobilities limited by different scattering mechanisms for a Si-implanted GaAs sample. The total mobility exactly coencides with the data (in small dots).

Since the implant energies for E514 and E522 were not very different from the other samples we may conclude that the measured high sheet concentration must be due to some other factor. Possibly the different annealing conditions for the samples E514 and E522, after implantation, helped to reduce the formation of Si_{Ga}-Si_{As} complexes. Thus offering higher activation of dopants, the available number of carriers would be higher.

The anomalous decrease and the increase of sheet carrier concentration with decrease in temperature cannot be explained easily. Two experiments were attempted in order to gain a better insight of the anomalous behavior. In the first, the substrate was thinned down from the back, but subsequent Hall measurements could not be performed due to uneven pressure of the probes breaking the samples. In the second experiment Au schottky diode were evaporated on the center of the implanted GaAs Hall samples and the Hall pads were isolated by scribing. A typical device is shown in Fig 4.5 The purpose was to apply a bias to the schottky contact and measure the sheet carrier concentration as a function of depth in the implanted layer. The effective thickness of the conducting layer is varied with varying bias. These measurements are in progress. At this point it may only be surmised that defects in the substrate or substrate-active layer interface are responsible for the observed behavior.

TABLE 4-1

Summary of parameters used for analysis
For Si-implanted GaAs

Parameters	Value
Θ ($^{\circ}$ K)	420
ρ (g/cm^3)	5.307
w_l (cm/s)	5.24E5
e_{14} (C/m^2)	0.16
E_1^{Γ} (eV)	8.6
$\frac{m_{\Gamma}^*}{m_o}$	0.067
C_{11} (dyne/cm^2)	11.88E11
C_{12} "	5.34E10
C_{44} "	5.94E11
ϵ_s	13.1
ϵ_d	11.1
a(Å)	5.6533

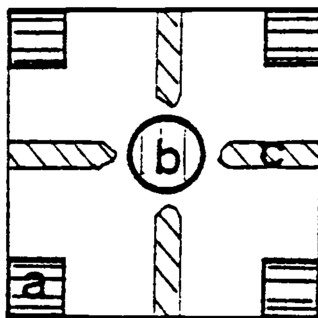

a) Ohmic contact
b) Schottky contact (4 to 5V of barrier height)
c) Fine scribe with a Tungsten tip

Fig 4.5 Technique tried to find the mobility in different regions of the implanted layer.

TABLE 4-2

Characteristics of Si-implanted GaAs from analysis of Hall data

Sample Number	From fabrication & measurement			From Analysis				
	Maximum mobility	Implant Dose (cm^{-2}) *	Mobility at 300K ($cm^2/V.s$)	N_D (cm^{-3})	N_A (cm^{-3})	$N_D - N_A$ (cm^{-3})	$\frac{N_D - N_A}{N_D + N_A}$	$N_s A$
E493	1750	3×10^{12}	1415	9.2E16	8.4E16	0.8E16	4.5%	3.5E5
E496	3550	5×10^{12}	2460	4.9E16	3.9E16	1E16	11.4 %	1.75E5
E499	3175	5×10^{12}	2270	4.32E16	3.7E16	0.62E16	7.7 %	2E5
E500	3600	3×10^{12}	2750	4E16	3.5E16	0.5E16	5.3 %	1.5E5
E503	3900	3×10^{12}	2800	4E16	3.2E16	0.8E16	11.1 %	1.45E5
E514	4600	3×10^{12}	2900	3.5E16	2.6E16	0.9E16	14.8 %	1.45E5
E522	3500	3×10^{12}	2400	3.5E16	3.06E16	0.44E16	6.7%	1.85E5
E578	2100	3×10^{12}	1660	9E16	7.5E16	1.5E16	9.1 %	2.9E5

* 140 keV

Chapter 5

Low and High Field Transport in $Al_xGa_{1-x}As$

5.1 Low Field Mobility

The measured variation of Hall mobility with temperature, and with composition at room temperature for samples with $0 < x \leqslant 0.6$ are shown in Figs 5.1 and 5.2, respectively. It is seen from Fig 5.1 that while the mobilities in samples with $x < 0.35$ are as expected, those in samples with $x \geqslant 0.35$ are about an order higher than those measured in liquid phase epitaxial (LPE) samples with the same composition. The low values of mobility for $x \geqslant 0.35$ depicted in Fig 5.2 were obtained after removal of the substrates in these samples. The difference in measured mobility upon removal of the substrate is highlighted in the data of Matsumoto et al (17) depicted in Fig 5.3. The measurements were made by these authors on similar OMVPE $Al_xGa_{1-x}As$ samples and the high values of mobilities were attributed by them to electron transfer from the epitaxial layer to the semi-insulating substrate.

The observed variation of Hall mobility with Al-content (shown in Fig 5.2) can be explained as follows. In the region $0 < x \leqslant 0.3$ the observed decrease in mobility can be almost totally explained by the increased polar optical phonon scattering which is the dominant scattering mechanism around 300K. The increased scattering is, in turn, due to increasing effective mass m^*_Γ of electrons which progressively moves up in energy in the Γ valley. In the band cross-over region $(0.3 < x \leqslant 0.5)$, significant carrier transfer to the subsidary minima

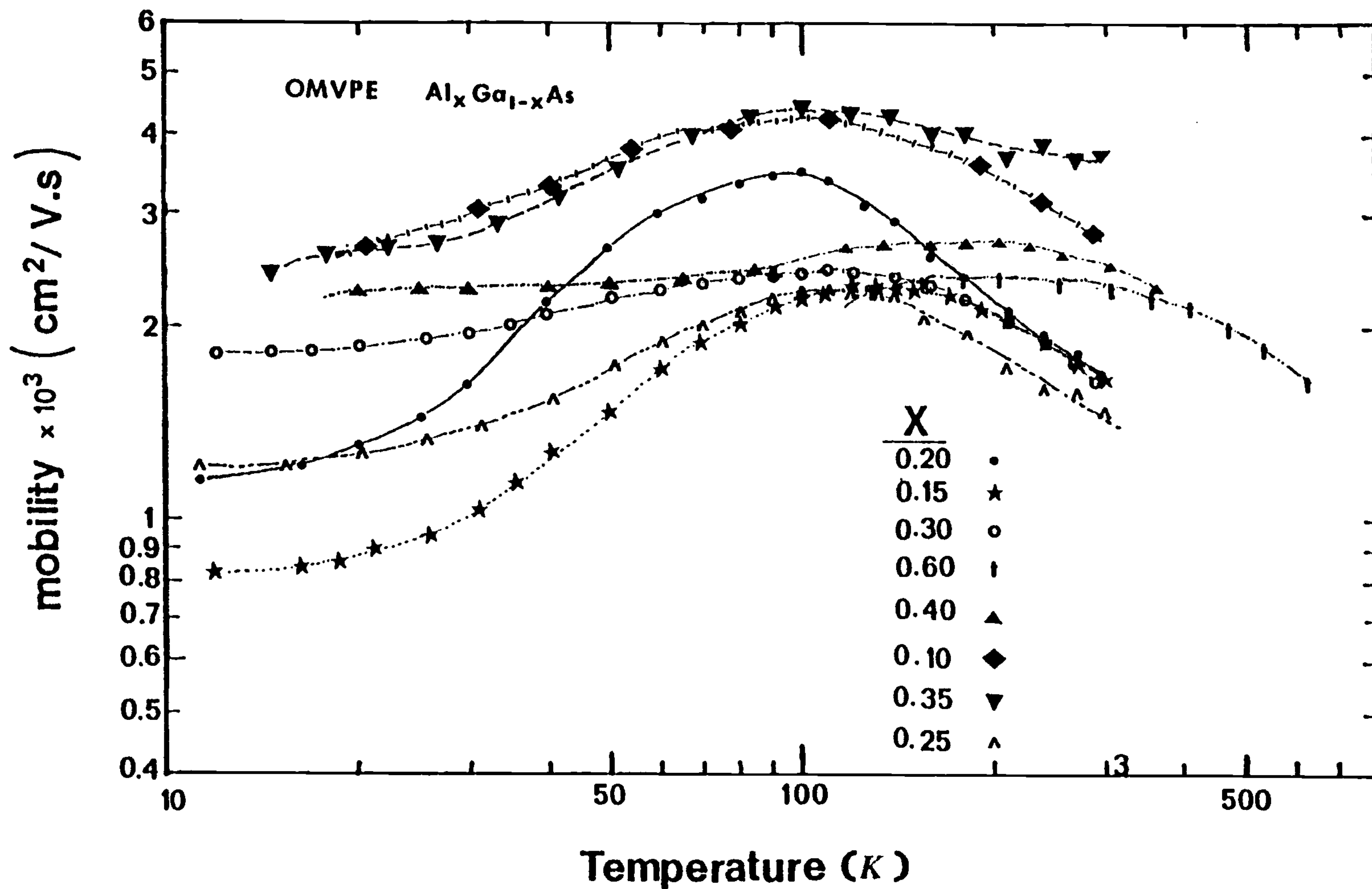

Fig 5.1 Measured variation of Hall mobility with temperature in undopd OMVPE $Al_xGa_{1-x}As$ for different alloy compositions.

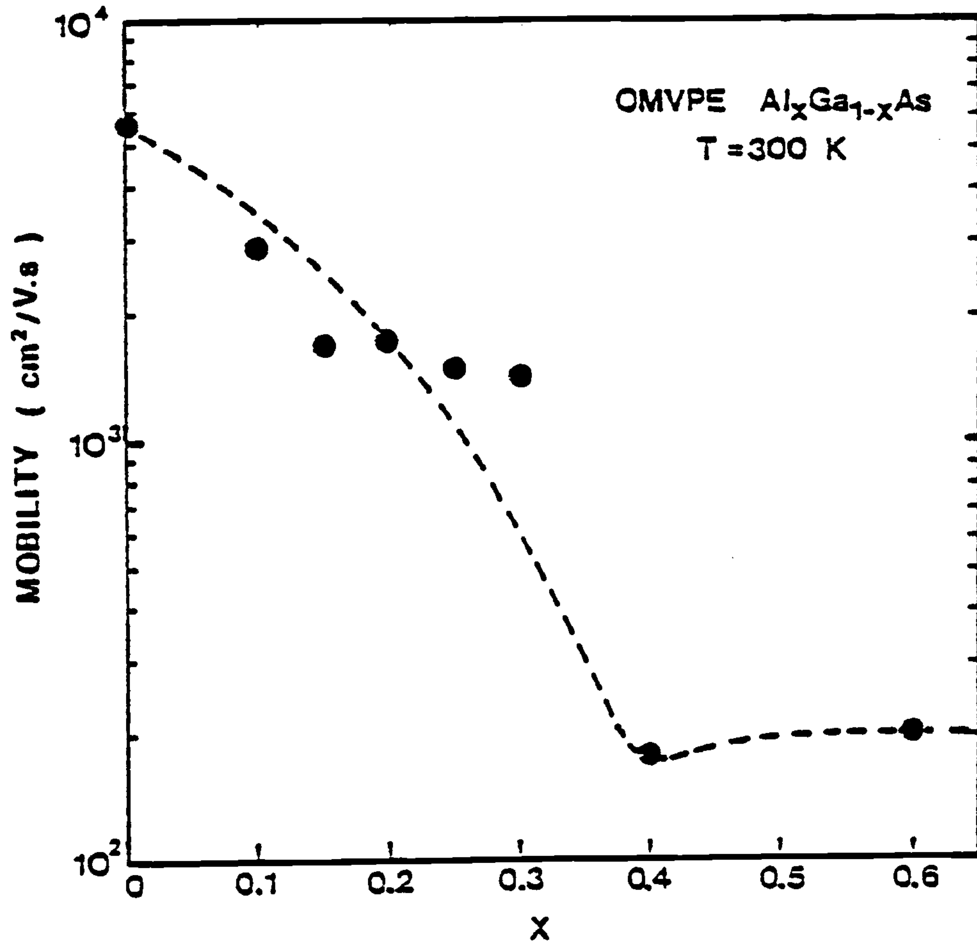

Fig 5.2 Measured variation of Hall mobility with composition at 300 K in undoped OMVPE $Al_xGa_{1-x}As$.

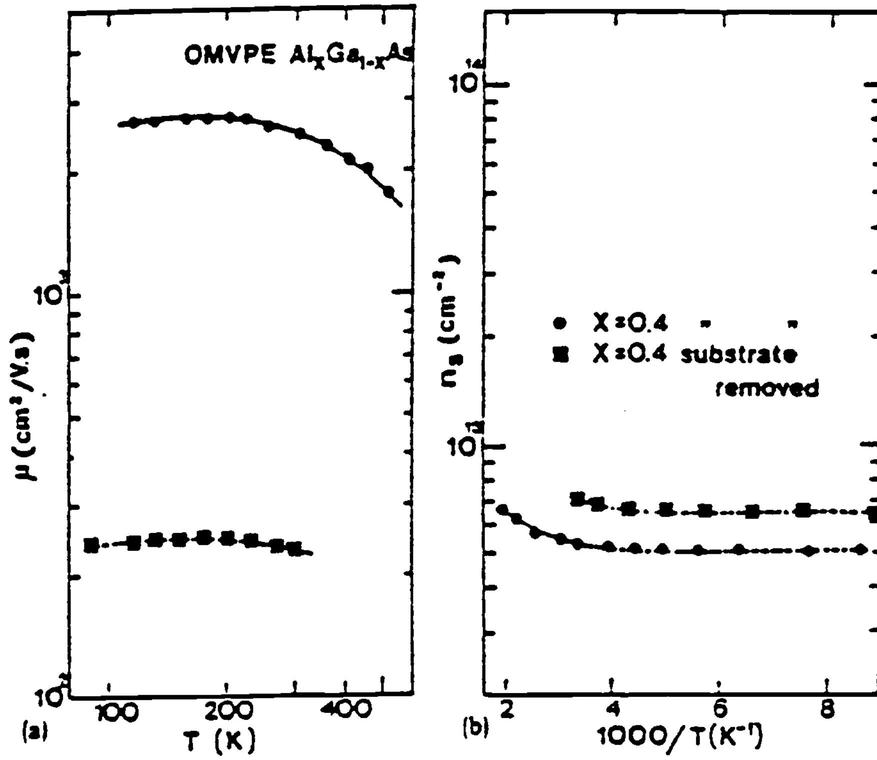

Fig 5.3 Temperature dependence of Hall electron mobility, μ , and sheet electron concentration, n_s, in OMVPE $Al_xGa_{1-x}As$ layers.

The solid lines indicate theoretical mobilities.

take place, causing a sharp fall in mobility value. For $x \geqslant 0.6$, the electrons reside mainly in the X minima, and the measured low values of mobility are indicative of the high electron effective mass in these minima. A minimum in mobility value usually occurs at $x \simeq 0.45$. This is due to a combination of intervalley, space charge and alloy scattering mechanisms. On comparison with electron mobility values in LPE $Al_xGa_{1-x}As$ with identical compositions and similar net donor densities, we find that the measured mobilities in OMVPE $Al_xGa_{1-x}As$ are less by a factor of 1.5. Photo luminescence (PL) measurements made on the same crystals by Bhattacharya et al [74] indicate that the PL intensities in the OMVPE crystals are slightly less than LPE crystals. These facts indicate higher compensation in OMVPE materials compared to LPE-grown crystals.

The temperature dependence of mobility in samples with different concentrations were analysed and the program used is given in appendix II. Figs 5.4, 5.5, 5.6 show the mobilities determined by different scattering mechanisms and their contribution to the total mobility.

Fig 5.7 shows the measured variation of Hall electron concentration n_H, with alloy composition at room temperature. Data of a limited number of samples, grown under similar conditions, have been presented here. The observed variation can be interpreted as follows. With increase of x , increasing number of carriers transfer to the subsidary minima which have high density of states and low mobilities, resulting in a lowered value of n_H. The minimum occurs at a composition slighly below the Γ-X cross over composition. With further increase of x, most of the electrons are in the X minima and n_H increases to

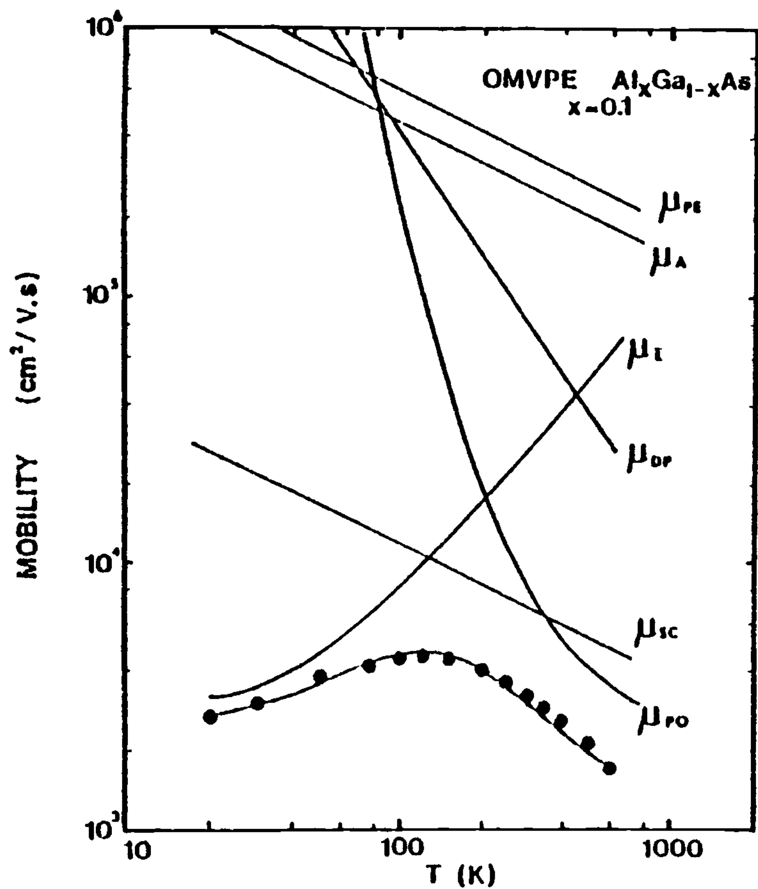

Fig 5.4 Variation of Hall mobility with temperature in undoped OMVPE $Al_{0.1}Ga_{0.9}As$. The solid line with the data indicates the calculated variation.

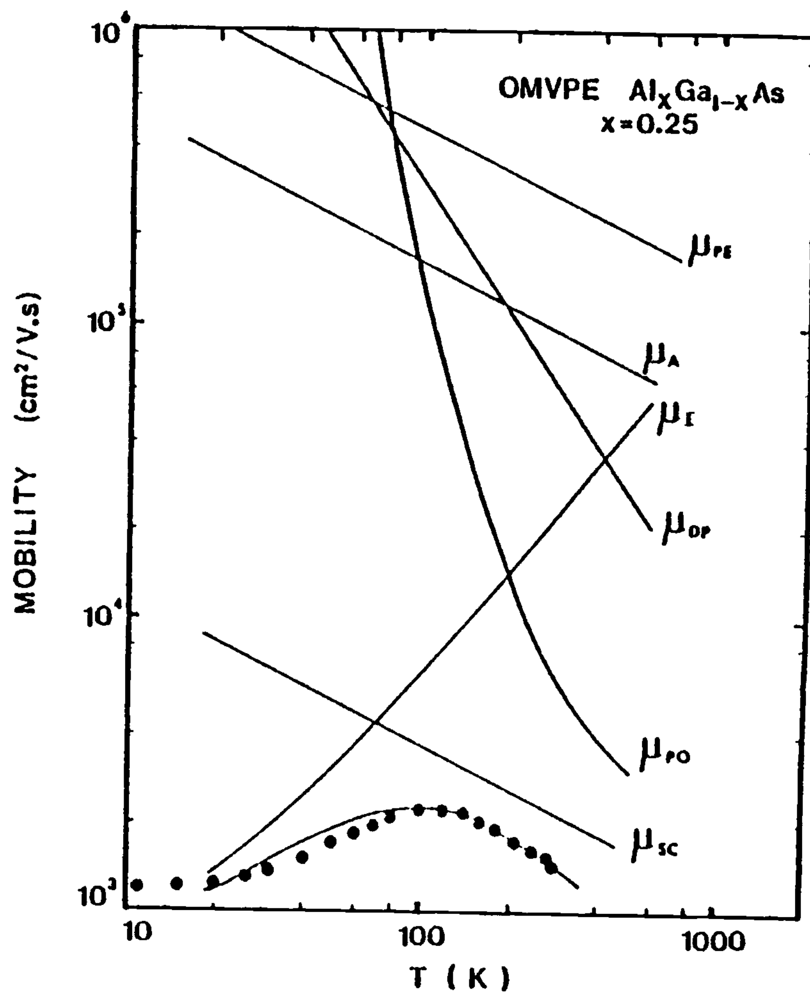

Fig 5.5 Variation of Hall mobility with temperature in undoped OMVPE $Al_{0.25}Ga_{0.75}As$. The solid line with the data indicates the calculated variation.

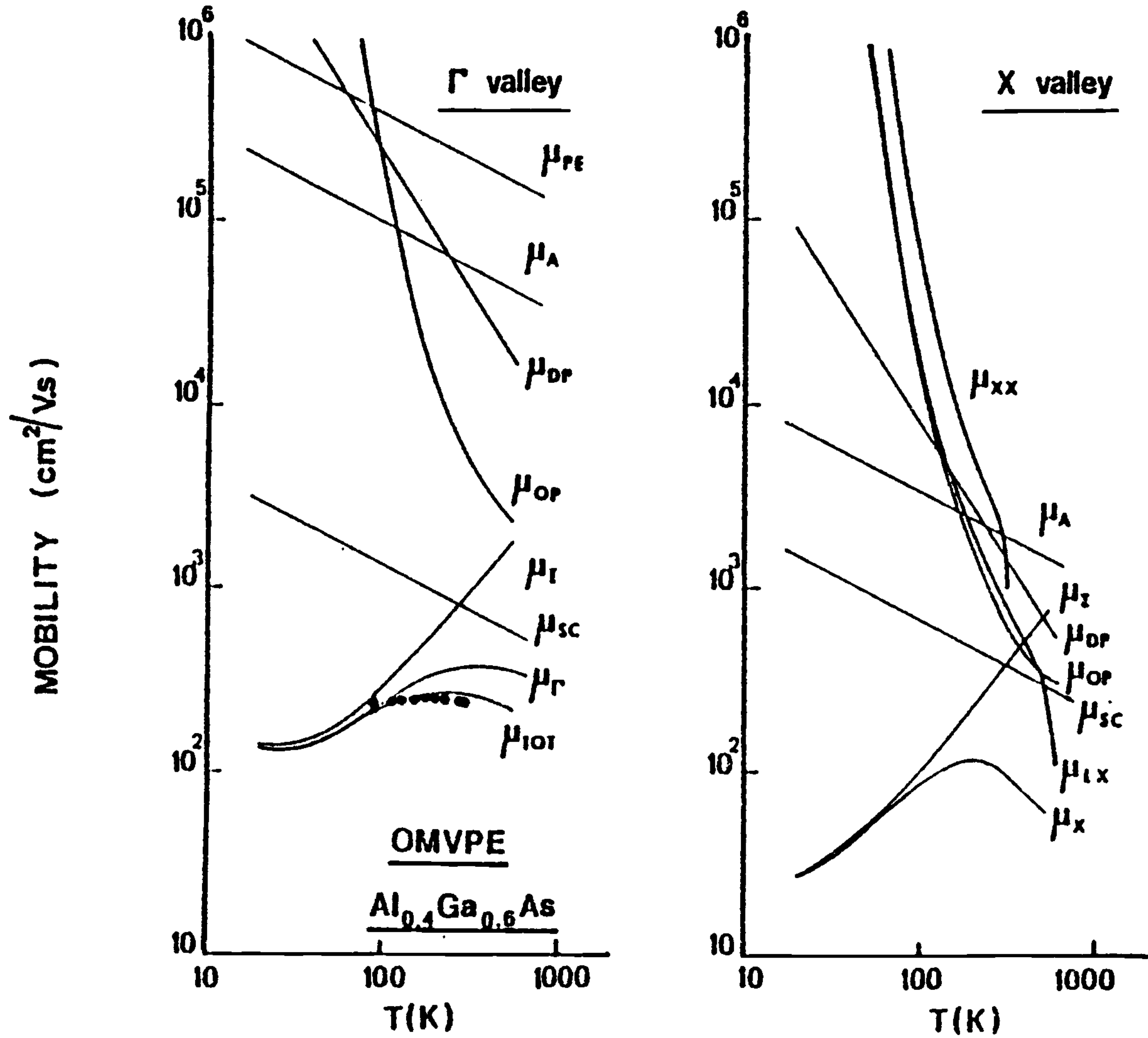

Fig 5.6 Electron mobilities limited by the different relevant scattering mechanisms in Γ and X minima $Al_{0.4}Ga_{0.6}As$. The solid line along side the data indicates the total calculated mobility.

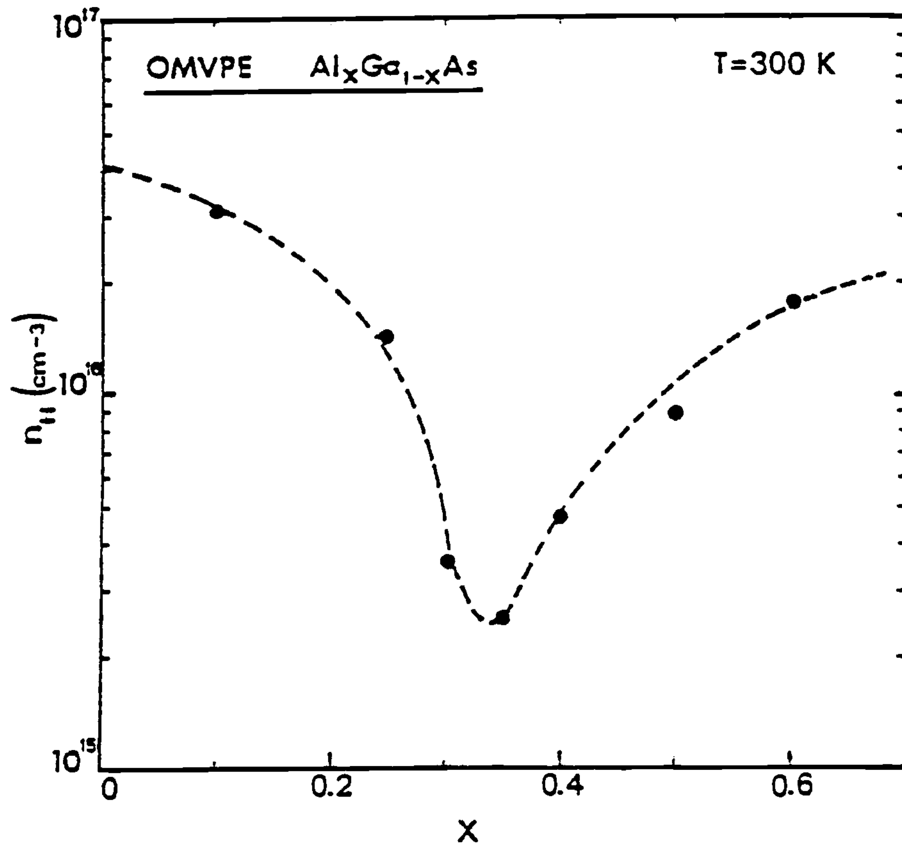

Fig 5.7 Measured variation of Hall electron concentration with composition at 300 K in undoped OVMPE $Al_xGa_{1-x}As$.

the value of the electron concentration in these minima.

The measured variation of n_H with temperature for the same samples were also analyzed with the charge neutrality equations given in Chapter 2 and the typical agreements with experimental data are shown in Figs 5.8 and 5.9 for undoped and Si-doped samples, respectively. The measured variation of n_H in a larger temperature range for some samples is shown in Fig 5.10. As in the case of Si-implanted GaAs it is seen that there is an identical anomalous variation of the carrier concentration at very low temperatures. In all these cases it was observed that the concentration levels-out to a constant value asymtotically to the lowest measured temperature of 11K.

It is known that a trap is associated with a certain amount of activation energy for carriers to get into the trap, and an amount of energy to escape from the trap. Photohall data of measurements done to explain the observations are presented in Fig 5.11. From these observations nothing can be particularily concluded, but since G. Robinson [76] has identified these types of traps in the Si-doped $Al_xGa_{1-x}As/GaAs$ layers it can be qualitatively said that at low temperatures the electrons donot have enough energy to get into the trap. This might show up in an increase in the hall carrier concentration at very low temperatures.

Results on Hall measurements performed at $T > 300$ K on some samples are shown in Fig 5.12. The energy values of deep levels and the position of the L minima obtained from the analysis of the measured variation of n_H with T are shown by the data points in Fig 5.13. Donor and acceptor level densities have also been derived from a

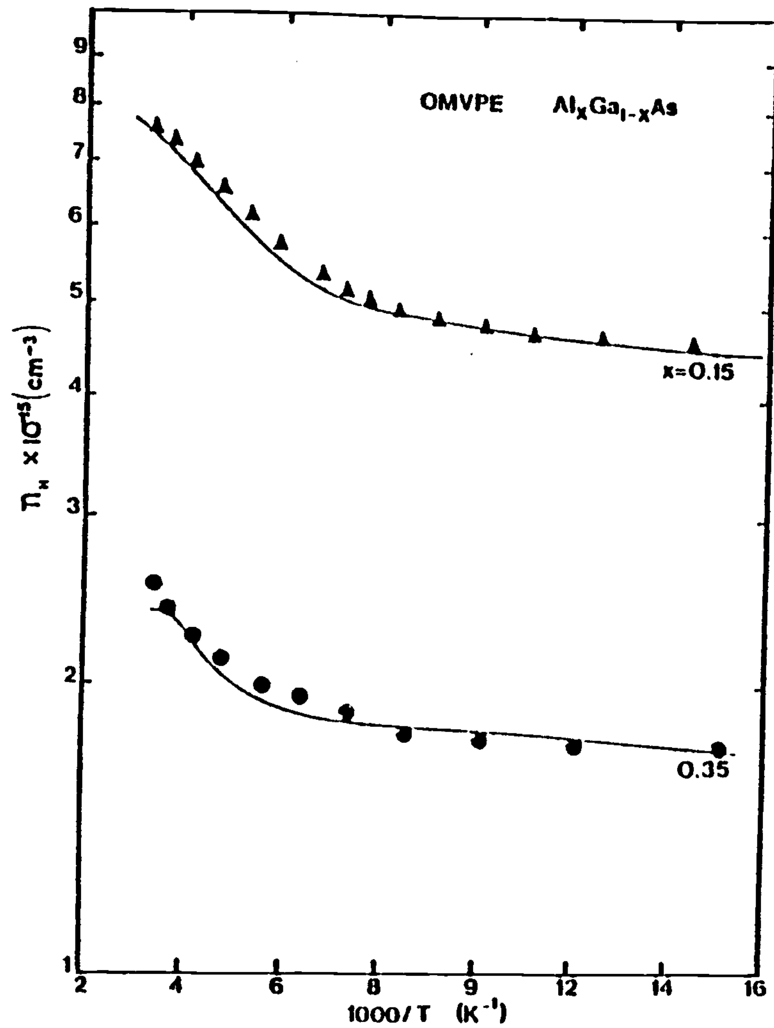

Fig 5.8 Measured and calculated variations of Hall electron concentration with temperature in undoped $Al_xGa_{1-x}As$ samples.

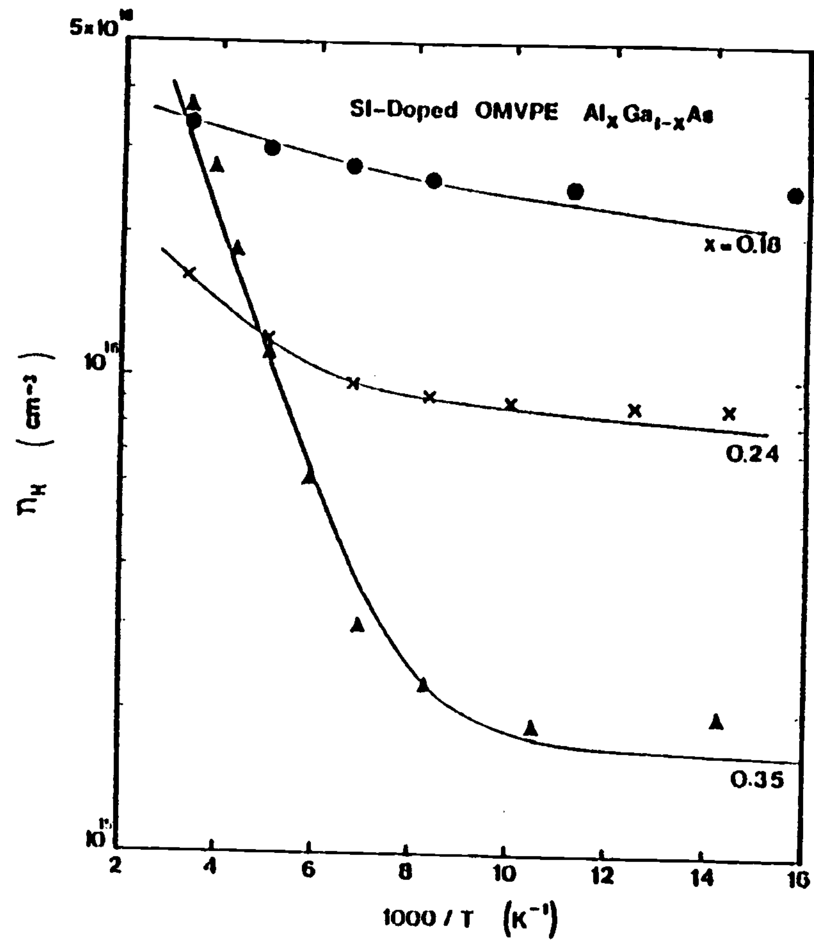

Fig 5.9 Measured and calculated variations of Hall electron concentration with temperature in Si-doped $Al_xGa_{1-x}As$ samples.

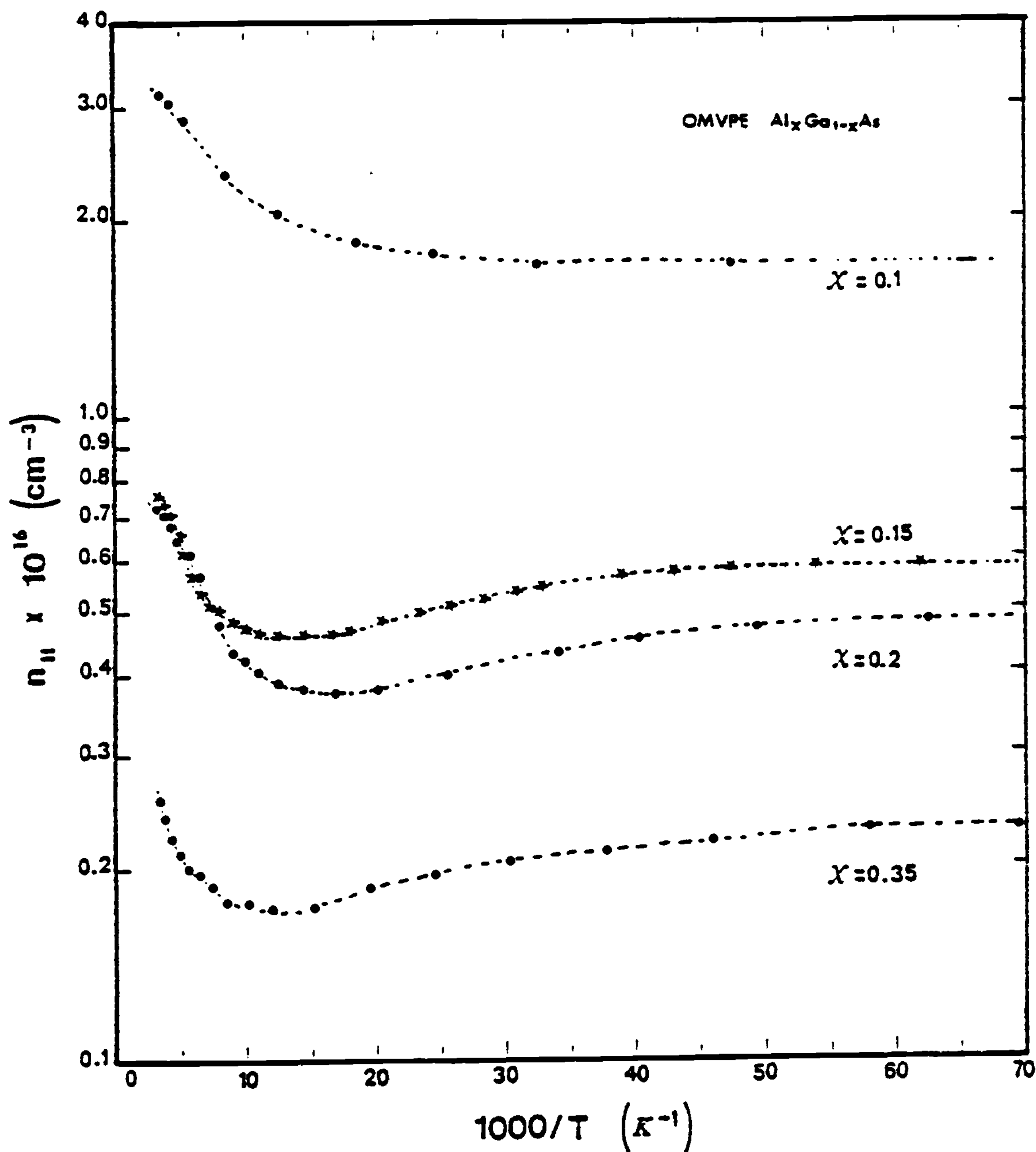

Fig 5.10 Measured variation of Hall electron concentration for undoped $Al_xGa_{1-x}As$ samples over a wide range of temperatures.

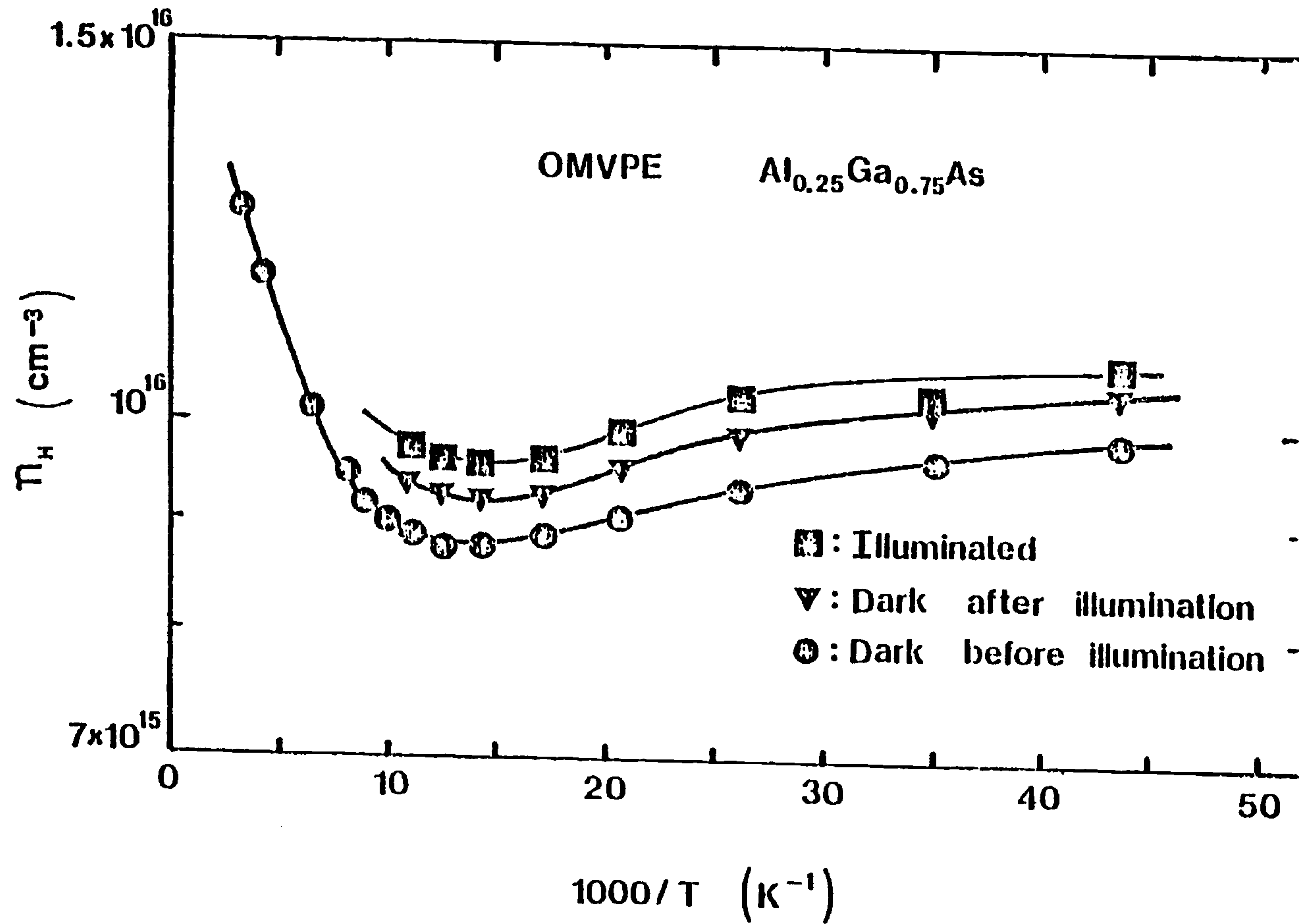

Fig 5.11 Variation of Hall concentration for photo-hall measurement with undoped $Al_{0.25}Ga_{0.75}As$.

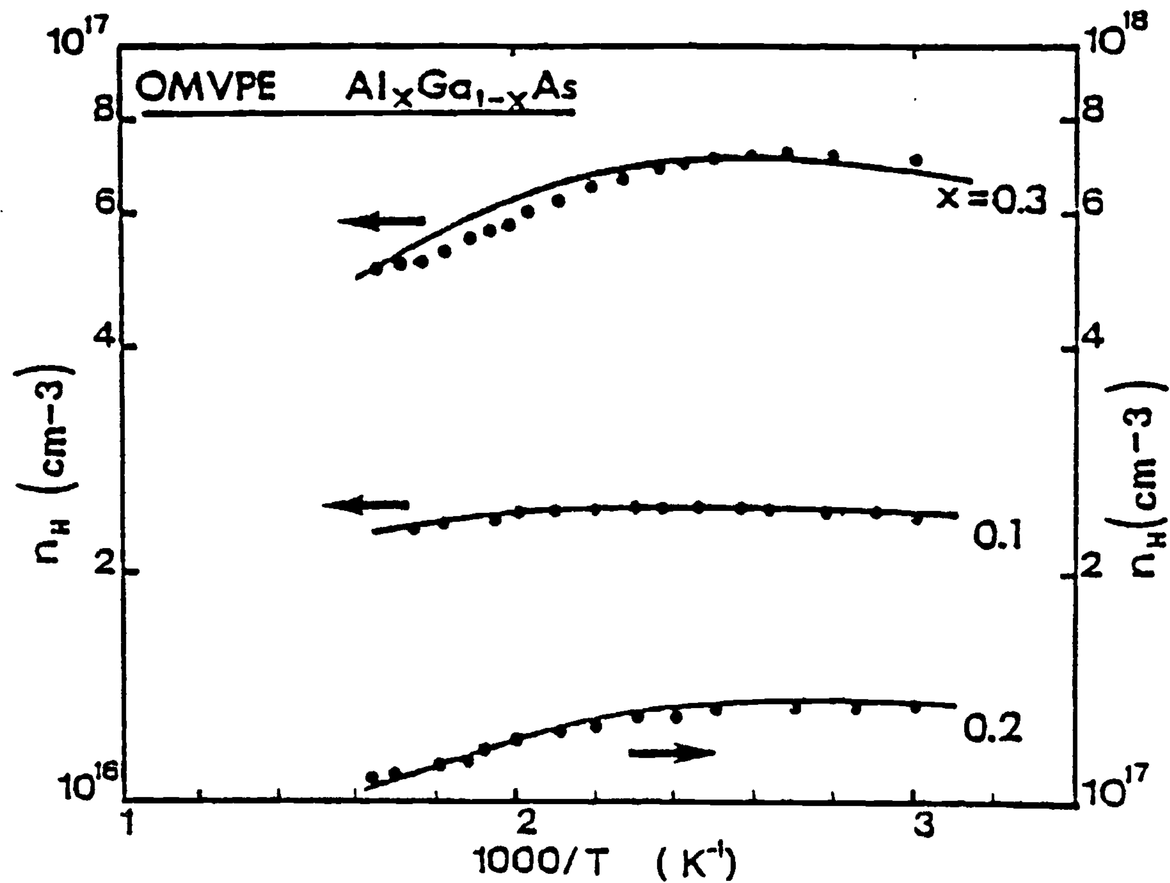

Fig 5.12 Measured and calculated variations of Hall electron concentration with temperature in undoped $Al_xGa_{1-x}As$ samples.

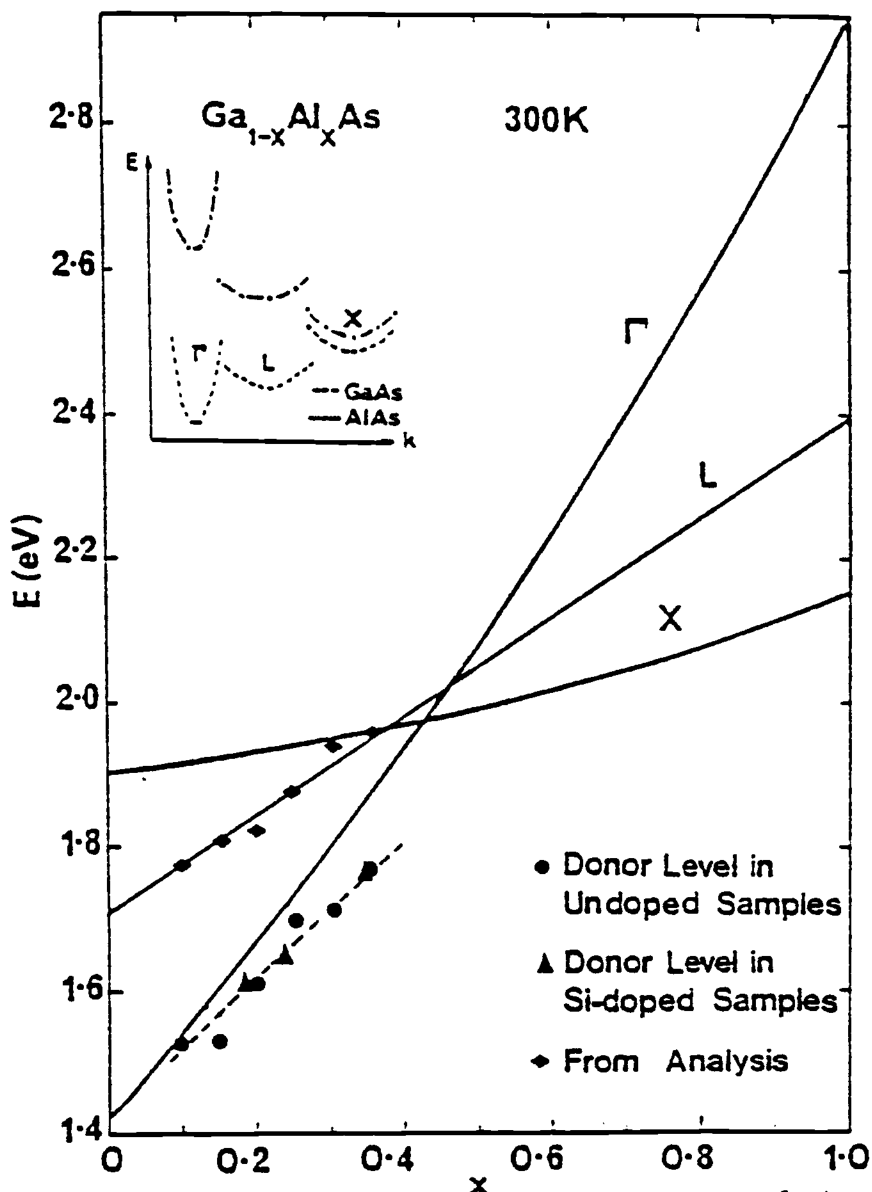

Fig 5.13 The data points for the energy position of the L minima and the donor levels determined in this study.

solution of the charge neutrality equation. The values of these densities are in good agreement with the corresponding values derived from analysis of mobility data. It is seen that there is a donor level in the undoped samples whose ionization energy increases from 0.025 to 0.113 e.V. in the composition range $0.15 \leqslant x \leqslant 0.35$. Ionization energies of Si-donors in the Si-doped samples were obtained from analysis are 0.022, 0.077 and 0.095 e.V., respectively, for x = 0.18, 0.24 and 0.35. The value of the donor ionization energy in Si-doped $Al_{0.24}Ga_{0.76}As$ is in good agreement with the value of 0.065eV in a similar composition estimated by Fischer et al [50] from photoluminescence pair-transition data. Like several other donor species in LPE $Al_xGa_{1-x}As$ [26, 71, 72], the activation energy of the donors in OMVPE samples also increases with increasing x. The increase can be explained by considering the interaction of the Γ, L and X wave functions near the band cross-over region.

The temperature variation of $\Delta_{\Gamma X}$ and $\Delta_{\Gamma L}$ have been taken into account. The program used for the analysis of Hall concentration data is outlined in Appendix III and the parameters used are summarised in Table 5.1. A summary of the measured data is shown in Table 5.2.

Values of N_sA, N_D and N_A required to obtain a good agreement of the calculated mobilities with data are listed in Table 5.3. Also listed are values of N_sA calculated by the emperical formula of Strigfellow et al [29]. The agreement is fair. Slightly higher values derived by us may reflect the influence of deep levels in the samples. The ratio μ_A/μ_{SC} that has been calculated from the fitting of mobility data is shown in Fig 5.14 for a limited composition range. It is clear

TABLE 5-1

Summary of parameters used for analysis of OMVPE $Al_xGa_{1-x}As$ Hall Data

$x \longrightarrow$	0.01	0.15	0.20	0.25	0.30	0.35	0.40
ρ (g/cm^3)	5.136	5.051	4.961	4.88	4.795	4.71	4.624
u_l (Km/s)	5.27	5.28	5.29	5.31	5.32	5.33	5.34
e_{14} (C/m^2)	0.16	0.16	0.16	0.16	0.16	0.16	0.16
E_1^{Γ} (eV)	8.5	8.5	8.6	8.6	8.6	8.6	8.5
E_1^{X} (eV)	5.2	5.5	5.8	6.4	7.0	7.5	8.6
$\left(\frac{m_{\Gamma}^*}{m_0}\right)$	0.073	0.076	0.079	0.082	0.085	0.088	0.091
c_l (dyne/cm^2)	1.405 E12	1.406 E12	1.407 E12	1.408 E12	1.409 E12	1.409 E12	1.411 E12
c_t (dyne/cm^2)	4.87 E11	4.87 E11	4.88 E11	4.88 E11	4.88 E11	4.88 E11	4.89 E11
ϵ_s	12.56	12.39	12.17	12.07	11.91	11.76	11.62
ϵ_∞	10.56	10.40	10.24	10.09	9.93	9.78	9.64
$\left(m_X^* / m_0\right)$	0.35	0.35	0.35	0.35	0.35	0.35	0.35
$\left(m_L^* / m_0\right)$	0.115	0.12	0.125	0.13	0.13	0.135	0.14
D_{XX} (eV)	3.7 E8	4.0 E8	4.3 E8	4.7 E8	5.5 E8	6.3 E8	6.8 E8
D_{LX} (eV)	3.7 E8	4.0 E8	4.3 E8	4.7 E8	5.5 E8	7.0 E8	9.25 E8
θ ($^\circ$K)	424	427	430	434	440	447	454
ΔU (eV)	0.3011	0.30165	0.3022	0.30275	0.3033	0.30385	0.3044

TABLE 5-2

Summary of the measured data for OMVPE $Al_xGa_{1-x}As$ samples.

Sample Number	X value	Thickness of epilayer in microns	Mobility at room temperature	Hall concentration at room temperature	Type
OM1169	0.10	10.2	3200	3.5E16	undoped
3OM805	0.15	3.32	1651	7.55E15	"
3OM804	0.20	3.07	1686	7.26E15	"
3OM798	0.25	3.27	1477	1.4E16	"
OM1171	0.30	8.60	1643	3.5E15	"
3OM383	0.35	3.47	3725	2.55E15	"
OM1180	0.40	9.8	240(without substrate)	7.78E15	"
3OM815	0.18	3.55	1459	3.39E16	Si-doped
3OM816	0.24	3.53	1610	1.62E16	"
3OM817	0.35	4.16	1100	3.65E16	"

<u>Table 5-3</u> Characteristics of Undoped and Si-doped OMVPE $Al_xGa_{1-x}As$ Obtained from Analysis of Hall Data.

Samples	x	N_D (x10^{16}) (cm^{-3})	N_A (x10^{16}) (cm^{-3})	Compensation Ratio $\left(\frac{N_D + N_A}{N_D - N_A}\right)$	N_s.A (cm^{-1})(x10^5) from analysis	N_s.A (cm^{-1})(x10^5) from Eqn. 13
OM 1169	0.10	3.8	2.7	5.9	1.2	0.7
3OM 805	0.15	1.0	0.3	1.9	2.4	1.0
3OM 804	0.20	4.3	3.6	11.3	1.6	1.3
3OM 798	0.25	1.8	0.1	1.1	3.0	1.6
OM 1171	0.30	0.54	0.04	1.2	2.6	2.0
3OM 815*	0.18	9.1	8.0	15.5	2.7	0.7
3OM 816*	0.24	8.3	7.3	15.6	2.0	1.3
3OM 817*	0.35	34.0	33.3	67.0	2.4	2.0

* Si-doped samples

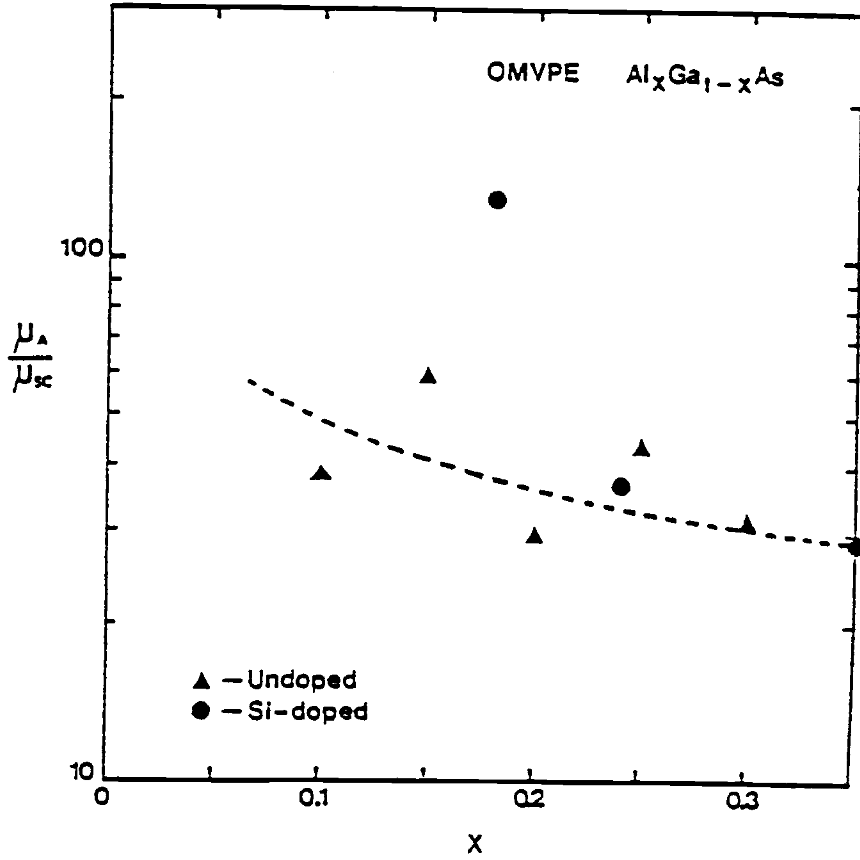

Fig 5.14 Ratio of mobilities limited by alloy and space-charge scattering. The symbols represent values drived from analysis of mobility data.

that the relative importance of alloy scattering, compared to scattering by space charge, increases with increasing x.

The calculated mobilities limited by alloy, space charge and intervalley scattering in the Γ and X minima for a limited composition range near band cross-over are depicted in Fig 5.15. The data points indicate the calculated values obtained from fitting of experimental results. It is evident that for x>0.3, L-X intervalley scattering has the most pronounced effect in lowering electron mobility.

5.2 High-Field Mobility

The measured variations of electron velocity with electric field at 300 K for samples with different concentrations are shown in Fig 5.16 (Ref: [67]). It is clear that the observed velocities in the sample with x = 0.4 is unusually large.

A typical potential versus distance plot is shown in Fig 5.17. These data for x = 0.6 at an elevated temperature was used to plot the velocity-field characteristics. Characteristics at 300 K and 400 K for a sample with x = 0.25 are shown in Fig 5.18. The inflection in the characteristics at 400 K has also been observed in $Al_{0.4}Ga_{0.6}As$ modulation doped hetrostructures [17] where it was attributed to real-space electron transfer from GaAs to $Al_xGa_{1-x}As$ at high fields. This process is depicted in Fig 5.19. In the epitaxial layer with x = 0.25 grown directly on a semi-insulating substrate, the velocities measured at room temperature are a combination of those for electrons in the ternary layer and of electrons which have transfered to the GaAs substrate. The major contribution to the velocity is, however, from the electrons in the termary layer. At room temperature the electrons

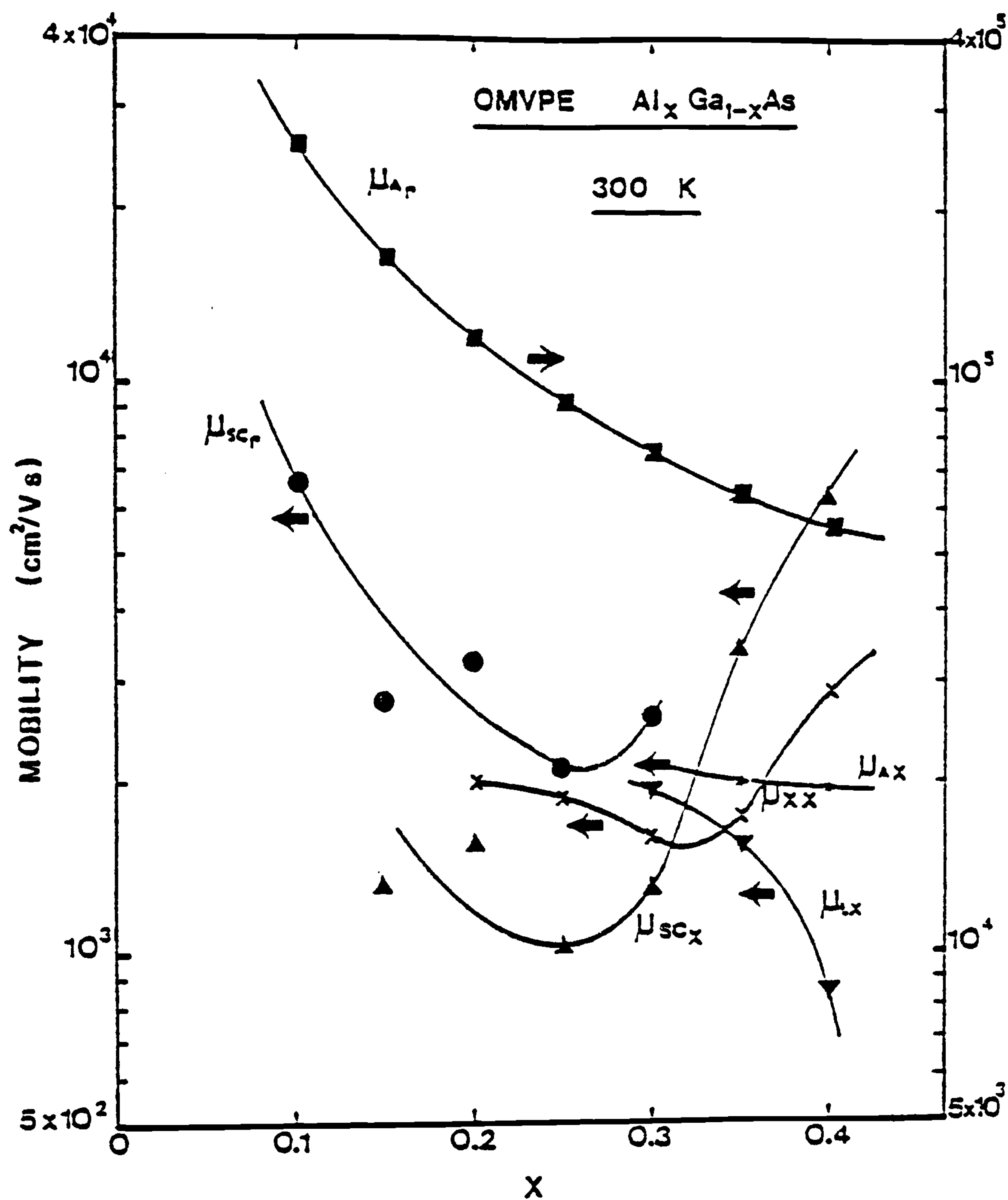

Fig 5.15 Mobilities in Γ and X valleys limited by alloy, space charge and intervalley scattering in $Al_xGa_{1-x}As$. The symbols represent values derived from analysis of mobility data.

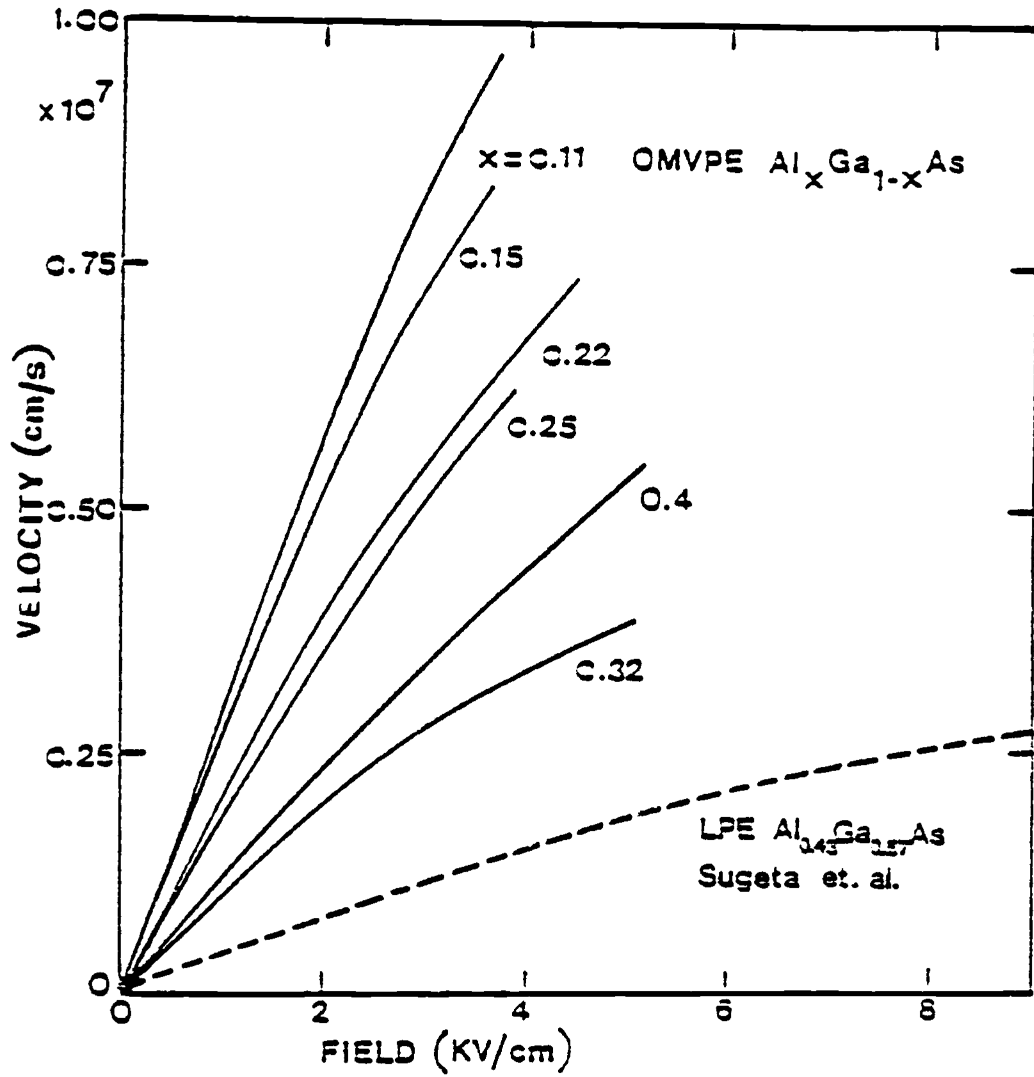

Fig 5.16 Velocity-field characteristics of electrons in OMVPE $Al_xGa_{1-x}As$ with 0   x   0.4.

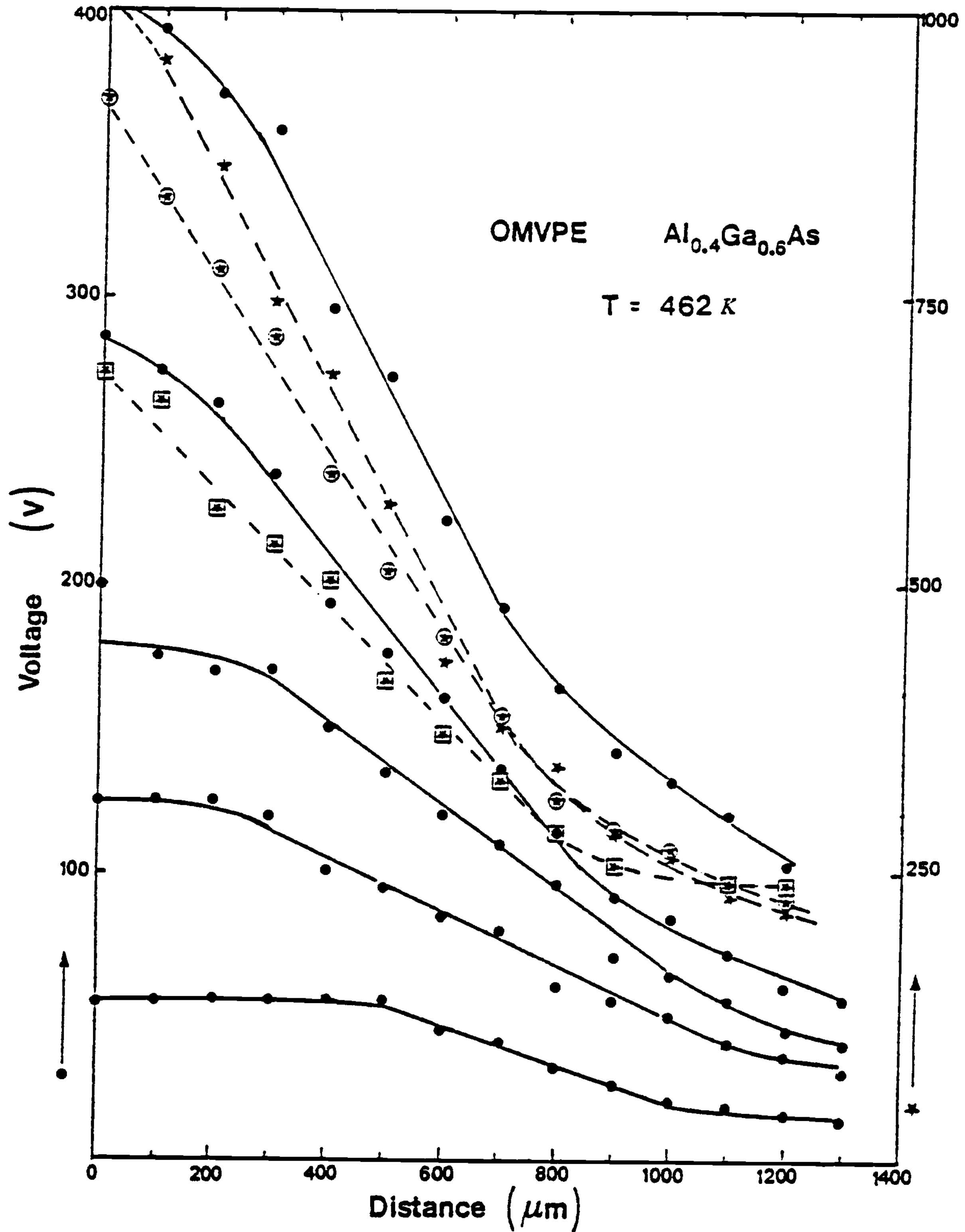

Fig 5.17 Potential distribution along the bridge of an H-device, fabricated on OMVPE $Al_{0.4}Ga_{0.6}As$.

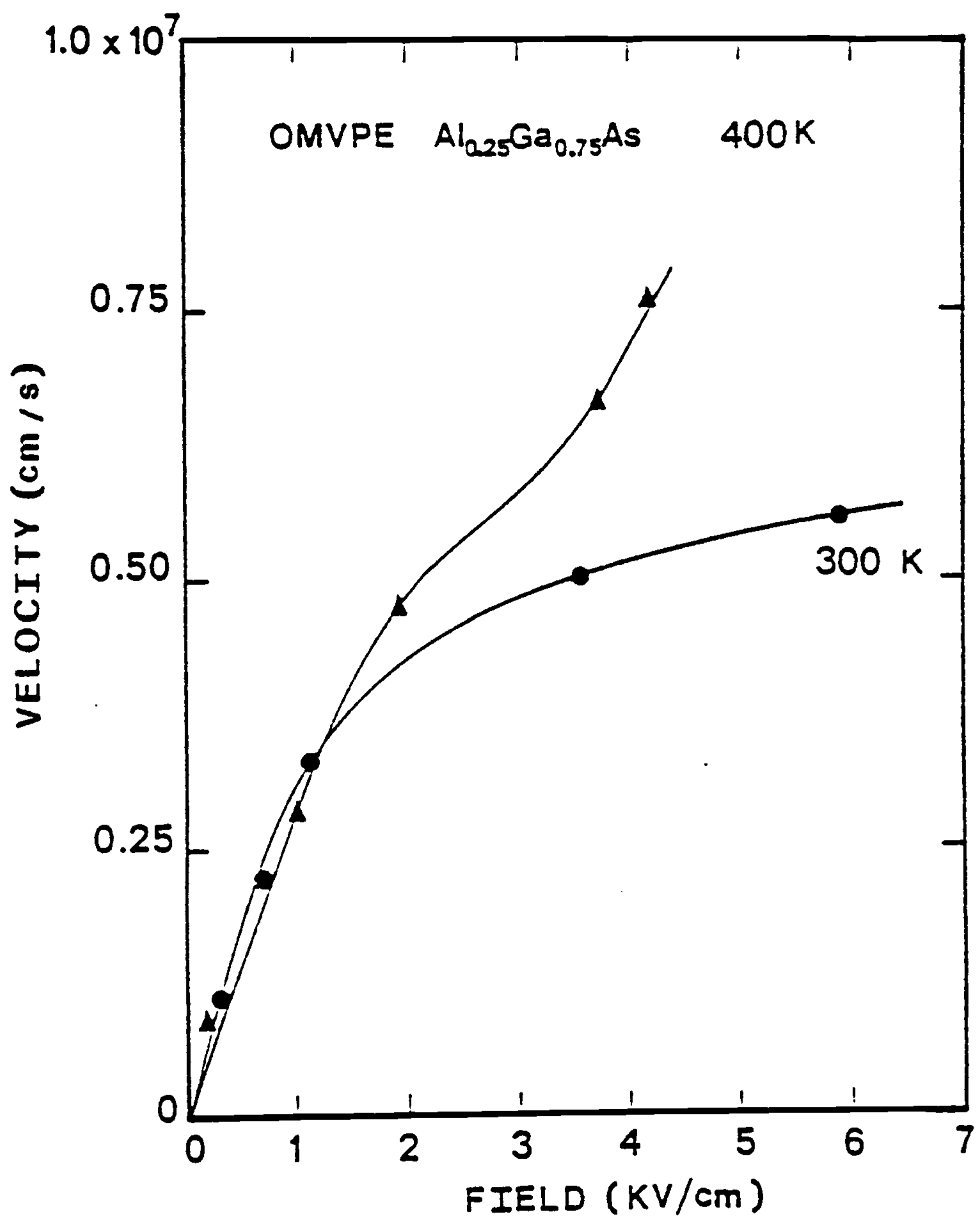

Fig 5.18 Velocity-field characteristics of electrons in $Al_{0.25}Ga_{0.75}As$ at 300 and 400 K.

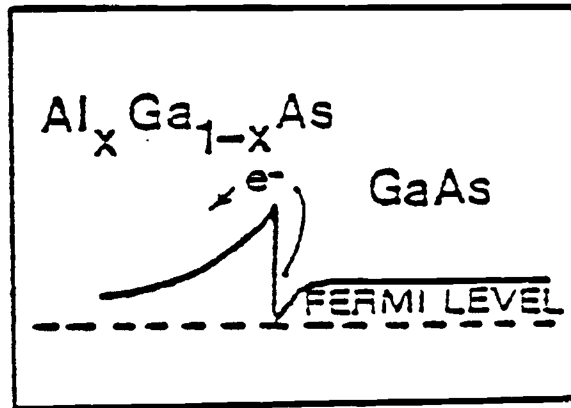

Fig 5.19 Process by which there is real-space electron transfer from the 2DEG to the $Al_xGa_{1-x}As$ epi layer at high applied electric fields.

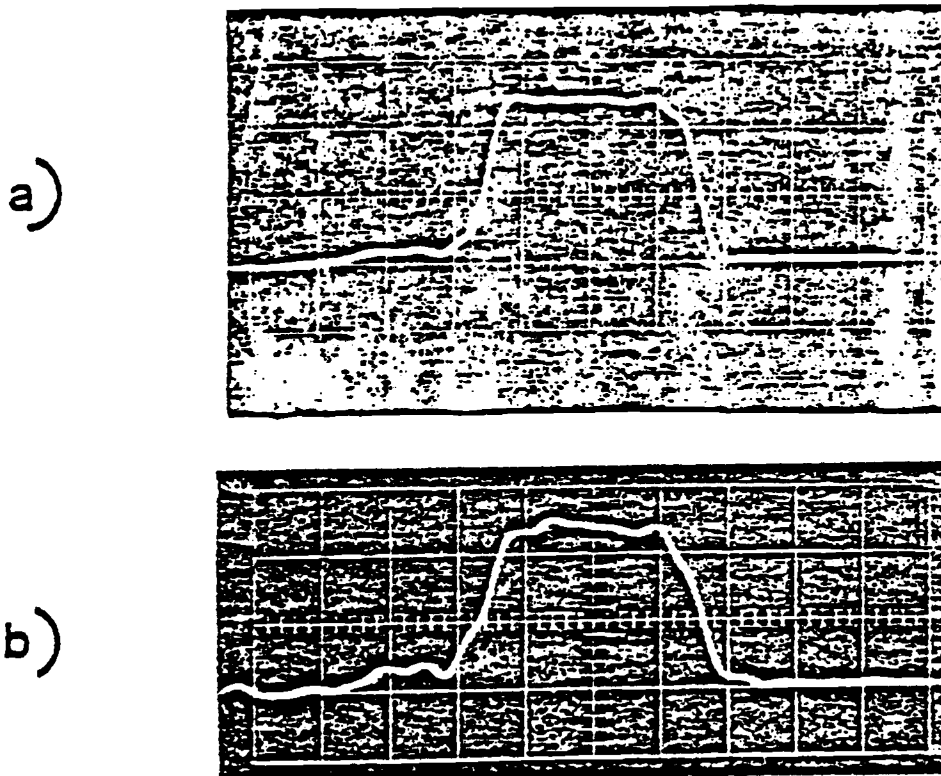

Fig 5.20 Effect of probe loading, current waveforms shown for sample 3om 383. (a) Without probe, y-axis is 5V/div, x-axis is 10ns/div. (b) With probe, y-axis is 5V/div, x-axis is 10ns/div.

in the GaAs layer cannot gain enough energy to surmount the hetro-structure barrier and be emitted into the ternary layer. It is quite probable that $\vec{k}$-space transfer of electrons from Γ to L-valleys in $Al_{0.25}Ga_{0.75}As$ would occur before real-space transfer, thereby causing a velocity saturation. At 400 K, the electrons in GaAs gain an extra amount of energy and therefore before real-space transfer, $\vec{k}$-space transfer is possible. From the analysis of the data in Fig 5.10 the values of $\Delta_{\Gamma L}$ (Fig 5.13) indicates that significant transfer starts only at T $\geqslant$ 500 K. However, the amount of inflection for x = 0.25 is too large and it should be observed below the 300 K characteristic.

Chapter 6

Conclusion

A detailed study of the transport properties in undoped and Si-doped OMVPE $Al_xGa_{1-x}As$ $(0 < x \leqslant 0.6)$ reveals that the roles of alloy, intervalley and space-charge scattering are predominant in limiting carrier mobilities. It is found that the sharp fall in the mobility at the band-crossover region is caused by equivalent and non-equivalent intervalley scattering. It was also found that the mobilities of OMVPE samples as compared to LPE samples of the same composition are less by a factor of approximately 1.5. This fact in conjunction with the lower PL intensities for OMVPE samples indicate higher compensation in OMVPE materials than in LPE-grown crystals.

The variation of the measured Hall electron concentration with temperature in $Al_xGa_{1-x}As$ has been analysed using a three-valley conduction band charge-neutrality model. It has been found that like several other donor species in LPE materials, the activation energy of the Si-donors in OMVPE samples also increases with increasing x. The increase can be explained by considering the interaction of the Γ, L and X wave functions near the band cross-over region. This increase of donor energies would be undesirable for device applications.

Although the anomalous variation of high-field drift velocity has been somewhat explained by involving modulation doping and real-space electron transfer, further work has to be done to establish the nature of process involved. In samples of higher resistivity where higher

voltages are required to give observable currents above the noise level, probe loading effects become pronounced. The same effects are observed during measurements at high temperatures. The loading effects can be minimized with a probe of resistance 1 MΩ or higher. Modifications of the sample holder are also necessary to make measurements below room temperature.

A more accurate evaluation of the L-valley mobility and other transport parameters is required. This would call for some exclusive experiments to evaluate the parameters of the L-valley.

The silicon implanted samples show a high level of compensation and one of the reasons for this could be the formation of Si_{Ga}-Si_{As} complexes. The compensation can be partly reduced by annealing the implanted substrates under higher As overpressures. Attempts to explain the increase of the carrier concentration at very low temperatures in both types of samples are in progress and modifications of the measurement set up are in progress.

Some measurements on back-gating effects of devices fabricated on identical or similar Si-implanted GaAs are in progress in this group. It may be recalled from earlier work [73] that oxygen implants compensate Si-implanted GaAs and provide uniform high resistivity isolation between active devices. Oxygen implants increase the backgating threshold voltage. This fact along with other temperature dependent measurements indicate that back-gating is determined essentially by a band of trap levels rather than a single deep level related to native defects. These results highlight the importance of experiments designed to gain a better understanding of the active layer-substrate interface.

Bibliography

1. M. Neuberger, Handbook of Electronic Materials, Vol 2, p 8, Data Corporation, New York (1971).

2. H.G. Casey and M. Panish, Hetrostructure Lasers, (Plenum, New York, 1978).

3. J.P. Andre, M. Boulon, P. Guittard and E. Roaux, : Proc. 8th Intern. Symp. on GaAs and Related Compounds, Viena, 1980, Inst. Phys. Cont. Ser. 56 (Inst. Phys., London, 1981) p 413.

4. D. Boccon-Gibord, J.P. Andre, P. Bandet and J. Hallais: IEEE Trans. Electron Devices, Ed-27 1141, (1980).

5. E. Fabre, A. Briere and J.P. Andre: Photovoltanic Solar Energy Conf., Luxembourg, 1977.

6. R.D. Dupuis, P.D. Dapkus, A.M. Garner, C.Y. Su and W.E. Spicer; Appl. Phys. Letters 34, 335, (1979).

7. S.J. Bass; J. Crystal Growth, 31, 172, (1975).

8. G.B. Stringfellow and G. Hom, Appl. Phys. Lett. 34, 794, (1979)

9. G.B. Stringfellow. J. Appl. Phys. 50, 4178, (1979).

10. G.B. Stringfellow and Linnebach. J. Appl. Phys. 51, 2212, (1980).

11. G.B. Stringfellow and H. Kunzel. J. Appl. Phys. 51, 3254, (1980).

12. E.E. Wagner, D.E. Mars, G. Hom and G.B. Stringfellow, J. Appl. Phys. 51, 5434, (1980).

13. E.E. Wagner, G. Hom and G.B. Stringfellow, J. Electron. Mater., 10, 239, (1981).

14. J. Hallais, J.P. Andre, A. Mircea-Roussel, M. Mahieu, J. Varon, M.C. Boissy and A.T. Vink, J. Electron. Mater. 10, 665, (1981).

15. N.M. Johnson, R.D. Burnham, D. Fekete and R.D. Yingling, Defects in Semiconductors (North-Holland, Amsterdam), 481, (1981).

16. T. Matsumoto, P.K. Bhattacharya, J. Darmawan and M.J. Ludowise; Int. Symp. GaAs and Related Compounds, Albuquerque, 1982 (Inst. Phys. Conf. Ser. No. 65: Chapter 4 pp. 289-296).

17. T. Matsumoto, P.K. Bhattacharya, J. Darmawan and M.J. Ludowise; Appl. Phys. Lett. 41, 1075 (1982).

18. R.D. Fairman, R.T. Chen, J.R. Oliver and D.R. Chen, IEEE Trans. Electron Devices, ED-28, 135 (1981).

19. H. Kanber, M. Feng, D.B. Ruby and G.E. Stillman, Presented at 23rd Electronic Matreials Conference, Santa Barbara, 1981.

20. K.L. Wang and G.P. Li, ibid.

21. R.S. Bhattacharya, A.K. Rai, Y.K. Yeo, P.P. Pronko, S.C. Ling, S.R. Wilson and Y.S. Park; J. Appl. Phys. 54, (1983).

22. A.K. Saxena, J. Phys. C. 13, 4323 (1980).

23. A.K. Saxena, Phys. Status Solidi (b) 105, 777 (1981).

24. A.K. Saxena, Int. J. Electron. 51, 779 (1981).

25. A.K. Saxena, P.K. Bhattacharya, A. Majerfeld; Int. Symp. on GaAs and Related compounds, p 199, St. Louis. (1979).

26. A.K. Saxena, Short Notes: Phys. Stat. Solidi (b) 96 K77 (1979).

27. B.R. Nag, in Theory of Electrical Transport in Semiconductors, (Pergamon, Oxford, 1972), p 187.

28. A.K. Saxena, Phys. Rev. B 24, 3295 (1981).

29. C. Erginsoy: Phys. Rev. 79, 1013 (1950).

30. N. Sclar, Phys. Rev. 104, (6), 1959 (1956).

31. B.R. Nag, Electron Transport in Compound Semiconductors Springer-Verlag, p 94, 1980.

32. H. Brooks, Advan. Electron. Electron Phys. 7, 158 (1955).

33. L.M. Falicov and M. Cuevas, Phys. Rev. 164 (3), 1025, (1967).

34. J. Bardeen and W. Shockley, Phys. Rev. 77, 407 (1950).

35. J. David Zook, Phy. Rev. 136, (3A), A869 (1964).

36. A. Fortini, J. Appl. Phys. 41, 3121 (1970).

37. L.R. Weisberg, J. Appl. Phys. 33 (5), 1817 (1962).

38. J.W. Harrison and J.R. Hauser, J. Appl. Phys. 47, 292 (1976).

39. J..W. Harrison and J.R. Hauser, Phys. Rev. B 9, 5347, (1976).

40. J.R. Hauser, M.A. Littlejohn and T.H. Glisson, Appl. Phys. Lett. 28, 458 (1976).

41. Shyh Wang, Solid State Electronics, McGraw Hill Co., 1966.

42. M.A. Littlejohn, J.R. Hauser, T.H. Glisson, D.K. Ferry and J.W. Harrison, Solid Stat. Electron. 21, 107, (1978).

43. Amitabh Chandra and L.F. Eastman, J. Appl. Phys. 51, (5), 2669, (1980).

44. A. Saxena and K.S. Gurumurthy J. Phys. Chem. Solids. 43 (9), 801, (1982).

45. C.W. Fawcett, A.D. Boardman and S. Swain, J. Phys. C, 31, 1963. (1970).

46. D.E. Aspnes, Phys. Rev. B 14, 5331 (1976).

47. J.L. Birman, M. Lax, and R. London, Phys. Rev. 145, 620 (1966).

48. M. Ilegems and G.L. Pearson, Phys. Rev 1, 1576 (1970).

49. K. Kaneko, M. Ayabe and N. Watanabe, Inst. Phys. Conf. Ser. 33a, 216 (1977).

50. P. Fischer, G. Kuhn, R. Bindemann, B. Rheinlander and W. Horig; Krist. Tech. 8, 167 (1963).

51. D.L. Rode, Phys. Status Solidi (b) 53, 245 (1972).

52. H.F. Mc-Skimin, F. Jayraman and P. Andreatch Jr., J. Appl. Phys. 8, 2362 (1967).

53. R.E. Fern and A. Outon, J. Appl. Phys. 42, 3499 (1971).

54. C.A. Mead and W.G. Spitzer, Phys. Rev. Lett. 11, 358 (1963).

56. A. Sagar, Phys. Rev. 117, 93 (1960).

57. B.B. Kosicki, A. Jayaraman and W. Paul, Phys. Rev. 172, 764 (1968).

58. J.S. Blackmore, Semiconductor Statistics, Pergamon Press, 1962.

59. M.A. Littlejohn, J.R. Haruser and T.H. Glisson, Appl. Phys. Lett., 30 (5), 242 (1977).

60. A. Majerfield, K.E. Potter and P.N. Robson, J. Appl. Phys. 45 (8), 3681 (1976).

61. T. Sugeta, A. Majerfeld, A.K. Saxena, P.N. Robson and G. Hill, Sixth Biennial Cornell Conference on Active Microwave Semiconductor Devices and Circuits, Ithaca, N.Y., 1977 (unpublished).

62. T. Sugeta, A. Majerfeld, A.K. Saxena and P.N. Robson, Appl. Phys. Lett. 31 (12), 842 (1977).

63. T.H. Windhorn, T.J. Roth, L.M. Zinkiewicz, O.L. Gaddy and G.E. Stillman, Appl. Phys. Lett. 40 (6), 513 (1982).

64. M. Keever, T.J. Drummond, H. Morkoc, K. Hess, B.G. Streetman and M.J. Ludowise; J. Appl. Phys. 53 (2), 1034 (1982).

65. T. Matsumoto, P.K. Bhattacharya, and M.J. Ludowise; Appl. Phys. Lett., 41 (7), 662 (1982).

66. T. Matsumoto, P.K. Bhattacharya, M.J. Ludowise; Appl. Phys. Lett., 42 (1), 52 (1983).

67. P. Banerjee, P.K. Bhattacharya, M.J. Ludowise and W.T. Dietze; IEEE Trans. Electron Device Lett., EDL-4, 283, (1983).

68. L.J. Van der Pauw, Phillips Research Reports, 13 (1), 1958.

69. V.G. Keramidas, H. Temkin, S. Mahajan; Inst. Phys. Conf. Ser., No. 56: Chap 5, pp 293, (1981).

70. V.L. Rideout, Solid State Electronics, 18, pp 541-550, (1975).

71. R.J. Nelson, Appl. Phys. Lett. 31, 351 (1977).

72. A.J. Spring Thorpe, F.D. King and A. Becke; J. Electron. Mater., 4, 101 (1975).

73. W.M. Paulson, M.S. Birrittella, T.H. Miers and McLaughin; "The effects of implanted Oxygen on backgating characteristics of GaAs IC's", GaAs IC Symposium, 166, (1982).

74. P.K. Bhattacharya, S. Subramanian and M.J. Ludowise, Journal of Applied Physics (submitted for publication).

75. G.B. Stringfellow, J. Crystal Growth, 53, pp 42-52, (1981).

76. Gary Robinson, (Dept. of Electrical Engg, University of Minnesota, Minneapolis) Graduate Seminar delivered at Oregon State University, Electrical Engg, Fall 1983.

Appendicies

Appendix I

Program for mobility analysis of Si-implanted GaAs

```
      PROGRAM HALL (INPUT,OUTPUT)
C IT CAN BE USED FOR BINARY, TERNARY OR QUARTENARY COMPOUNDS.
C THIS PROGRAM CALCULATES THE MOBILITIES AFFECTED BY
C VARIOUS SCATTERING MECHANISMS
      INTEGER I,K
      REAL UI(25),UPE(25),UPO(25),UA(25),UDP(25),USC(25),UNI(26),
     C T(26),UTOT(25),EPSO,B(25),THETA
      COMMON XND,XNA,XNO,XNSA,DELTU
      COMMON/ONE/ RHO,WL,D14,ADP,CL,CT,EPSS,EPSD,REMAS,RAD,XNUM(25),
     C G(25),X,L,M
      CHARACTER ANS*3
C NUM=G(THETA/T), IS FORTINI*S FUNCTION
C INITIALIZATION
C L IS FLAG FOR ALGAAS OPTION
C M IS FLAG FOR TEMPERATURE RANGE OPTION
      EPSO=8.854E-12
C ENTERING ALL THE NECESSARY PARAMETERS
    1 WRITE (*,5)
    5 FORMAT (≠PLEASE ENTER ALL THE NECESSARY PARAMETERS FOR THIS MATERI
     CAL AND YOU ARE WELCOME TO THIS PROGRAM≠)
      PRINT*,*IT CALCULATES THE MOBILITIES IN TEMPERATURE RANGE OF 20 TO
     C 540 KELVIN*
   10 PRINT*,*ENTER THE PHONON TEMPERATURE OF THIS MATERIAL(THETA) IN DE
     CGREE KELVIN*,
   15 READ(*,*) THETA
   16 PRINT *,*DO YOU WANT TO CANCEL THETA VALUE, YES OR NO*,
      READ (*,*(A)*) ANS
      IF (ANS .NE. *YES* .AND. ANS .NE. *NO*) GO TO 16
      IF (ANS .EQ. *YES*) GO TO 10
      M=0
   21 PRINT*,*DO YOU WANT TO START FROM 20 TO 540, YES OR NO**,
      READ(*,*(A)*)ANS
      IF (ANS .NE. *YES* .AND. ANS .NE. *NO*) GO TO 21
      IF (ANS .EQ.*YES*) GO TO 23
      T(1) =50.0
      DO 22 I =1,18
        DT = 0.15 * T(I)
        T(I+1)= T(I)+DT
        G(I)=THETA/T(I)
   22 CONTINUE
      M=1
      GO TO 30
   23 T(1)=20.0
      DO 24 I=1,25
        DT=0.15*T(I)
        T(I+1)= T(I) +DT
        G(I)= THETA/T(I)
   24 CONTINUE
   30 L=0
   33 PRINT*,*IS THIS FOR ALGAAS-YES OR NO*,
      READ(*,*(A)*)ANS
      IF (ANS .NE. *YES* .AND. ANS .NE. *NO*) GO TO 33
      IF (ANS .EQ. *YES*) THEN
         L=1
      ENDIF
   35 CALL ENTER
   36 PRINT*,*DO YOU WANT TO CANCEL THE PARAMETERS-YES/NO*,
      READ(*,*(A)*) ANS
      IF (ANS .NE. *YES* .AND.ANS .NE. *NO*) GO TO 36
      IF (ANS .EQ. *YES*) GO TO 35
C CALCULATIONS OF THE MOBILITIES
   40 CALL XENTR
   44 PRINT*,*DO YOU WANT TO CANCEL THE FITTING PARAMETERS-YES/NO*,
```

```
      READ(*,*(A)*) ANS
      IF (ANS .NE. *YES* .AND. ANS .NE. *NO*) GO TO 44
      IF (ANS .EQ. *YES*) GO TO 40
   42 WRITE(*,43)
   43 FORMAT (≠  TEMP.   ION.IMPR.   ALLOY SC.   DEFORM.P.   SP. CHAR.   PIEZO
     C ELC.   OPT.PHON.   UNI.MOBL.   TOT.MOBL.≠)
      IF (M .EQ. 1) THEN
         K=18
      ELSE
         K=25
      ENDIF
      XNN = XND + XNA
   45 DO 95 I=1,K
C CALCULATION OF THE B FACTOR
   50 B(I)=1.29E14*REMAS*EPSS*(T(I)**2)/(XND-XNA)
C CALCULATION OF THE IONIZED IMPURITY SCATTERING MOBILITY
   55 UI(I)=3.28E15*(EPSS**2)*(T(I)**1.5)/((2.*XNA+XND)
     C*(LOG(B(I)+1.)-(B(I)/(B(I)+1.)))*(REMAS**.5))
C CALCULATION OF OPTICAL PHONON MOBILITY
   60 UPO(I)=25.4*(T(I)**0.5)*(EXP(G(I))-1)*XNUM(I)/((1./EPSD-
     C1./EPSS)*(REMAS**1.5)*THETA)
C CALULATION OF THE ALLOY      MOBILITY , STATEMENT 65 IS A DUMMY STATEMENT
   64 IF (L .EQ. 1) GO TO 67
   65 UA(I)=9.43E3/((T(I)**0.5)*(REMAS**2.5)*(DELTU**2)*(RAD**3))
   66 GO TO 70
C THIS IS ALLOY MOBILITY CALCULATION FOR ALGAAS
   67 UA(I)= 52.83/((T(I)**0.5)*(REMAS**2.5)*X*(1. -X)*(DELTU**2))
C CALCULATION OF THE DEFORMATION MOBILITY
   70 UDP(I)=(3.17E-5*RHO*(WL**2))/((T(I)**1.5)*(ADP**2)*(REMAS**2.5))
C CALCULATION OF THE PIEZOELECTRIC MOBILITY
   75 UPE(I)=2.52E12/((T(I)**0.5)*(REMAS**1.5)*((Q14/(EPSS*
     CEPSO))**2)*((4./CT)+3./CL))
C CALCULATION OF SPACE CHARGE SCATTERING MOBILITY
   80 USC(I)=3.2E9/((T(I)**0.5)*(REMAS**0.5)*XNSA)
C  CALCULATION OF NEUTRAL IMPURITY SCATTERING MOBILITY (DAS)
   83 UNI(I) = ((1.17E22*REMAS)/(EPSS*8.859E-12*XNN)) *
     C  (7.34E-3*EPSS*8.859E-12*T(I)**0.5/REMAS**0.5 + 30.2*REMAS**
     C  0.5/(EPSS*8.859E-12*T(I)**0.5))
C CALCULATION OF THE TOTAL MOBILITY
   81 UTOT(I)=(1./UPE(I)+1./UPO(I)+1./USC(I)+1./UI(I)+1./UA(I)+
     C1./UDP(I) + 1./UNI(I))**(-1)
   85 WRITE(*,90)T(I),UI(I),UA(I),UDP(I),USC(I),UPE(I),UPO(I),UNI(I),
     C  UTOT(I)
   90 FORMAT (* *,F5.1,2X,E9.3,2X,E9.3,2X,E9.3,2X,E9.3,2X,E9.3,
     C 2X,E9.3,2X,E9.3,2X,E9.3)
   95 CONTINUE
  100 PRINT*,*DO YOU WANT TO CHANGE THE MATERIAL - YES OR NO***,
  105 READ(*,*(A)*)ANS
  110 IF(ANS .NE.*YES* .AND. ANS.NE. *NO*) GO TO 100
  115 IF (ANS .EQ. *YES*) GO TO 10
  120 PRINT*,*DO YOU WANT TO CHANGE THE FITTING PARAMETERS-YES OR NO**,
  125 READ(*,*(A)*) ANS
  130 IF (ANS .NE.*YES* .AND. ANS .NE. *NO*) GO TO 120
  135 IF (ANS .EQ. *YES*)GO TO 40
  140 PRINT*,*THIS IS THE END OF THE PROGRAM, GOOD LUCK****
  145 STOP
  150 END
C THESE ARE THE SUBROUTINES TO ENTER THE DATA PARAMETERS
        SUBROUTINE ENTER
        COMMON/ONE/ RHO,WL,Q14,ADP,CL,CT,EPSS,EPSD,REMAS,RAD,XNUM(25),
     C G(25),X,L,M
        IF (M .EQ. 1) GO TO 4
        DO 3 I=1,25
```

```
        PRINT*,*ENTER THE VALUE OF G(THETA) FOR THETA/T=*,G(I)
        READ(*,*) XNUM(I)
  3     CONTINUE
      GO TO 10
  4   DO 5 I=1,15
        PRINT*,*ENTER THE VALUE OF G(THETA) FOR THETA/T=*,G(I)
        READ(*,*) XNUM(I)
  5   CONTINUE
 10   PRINT*,*ENTER THE MASS DENSITY IN GRAM PER  CM3*,
 15   READ(*,*) RHO
 20   PRINT*,*ENTER THE VELOCITY OF SOUND IN THAT MATERIAL IN CM PER SE
     CCOND*,
 25   READ(*,*) WL
 30   PRINT*,*ENTER THE PIEZOELECTRIC CONSTANT (E14) IN COULOMB PER M2
     C *,
 35   READ(*,*) Q14
 40   PRINT*,*ENTER THE ACOUSTIC DEFORMATION POTENTIAL IN ELECT.VOLT*,
 45   READ (*,*) ADP
 50   PRINT*,*ENTER THE RELATIVE EFFECTIVE MASS*,
 55   READ (*,*) REMAS
 60   PRINT*,*ENTER THE LONGITUDINAL ELASTIC CONSTANT IN DYNE/CM2*,
 65   READ (*,*) CL
 70   PRINT*, *ENTER THE TRANSVERSAL ELASTIC CONSTANT IN DYNE PER CM2*,
 75   READ (*,*) CT
 80   PRINT*, *ENTER THE LOW FREQUENCY DIELECTRIC CONSTANT,EPSS*,
 85   READ (*,*) EPSS
 90   PRINT*, *ENTER THE HIGH FREQUENCY DIELECTRIC CONSTANT,EPSD*,
 95   READ (*,*) EPSD
 99   IF (L .EQ. 1) GO TO 110
100   PRINT *,*ENTER THE LATTICE CONSTANT IN ANGSTROMS*,
105   READ (*,*) RAD
106   GO TO 120
110   PRINT *,*ENTER THE X VALUE OF AL GA AS*,
115   READ (*,*)X
120   RETURN
      END
C
C
      SUBROUTINE XENTR
      COMMON XND,XNA,XNO,XNSA,DELTU
  10  PRINT *, *ENTER ND IN CM-3*,
  20  READ (*,*) XND
  30  PRINT*, *ENTER NA PER CM3*,
  40  READ (*,*) XNA
  50  PRINT *, *ENTER NO PER CM3*,
  60  READ (*,*) XNO
  70  PRINT*, *ENTER THE ALLOYING POTENTIAL IN ELECTRON VOLTS*.
  80  READ (*,*) DELTU
  90  PRINT*,*ENTER NS.A IN CM-1*,
 100  READ (*,*)XNSA
      RETURN
      END
```

Appendix II

Program for mobility analysis of $Al_xGa_{1-x}As$ in a wide range of alloying compositions

```
      PROGRAM HALL (INPUT,OUTPUT)
C IT CAN BE USED FOR BINARY, TERNARY OR QUARTENARY COMPOUNDS.
C THIS PROGRAM CALCULATES THE MOBILITIES AFFECTED BY
C VARIOUS SCATTERING MECHANISMS
      INTEGER I,K
      REAL UI(25),UPE(25),UPO(25),UA(25),UDP(25),USC(25),UNI(26),
     C T(26),UTOT(25),EPSO,R(25),THETA
      REAL RX(25),UPOX(25),UAX(25),UDPX(25),UPEX(25),USCX(25)
      REAL UNIX(25),APPU(25),DEC(25),BXX(25),RXX(25),UXX(25),BEC(25),
     C BLX(25)
      REAL ULX(25),UTOTX(25),UTOTL(25),RNL(25),RMX(25),RUL(25),PUX(25)
      REAL UAV(25),UH(25),RLX(25),UIX(25)
       REAL ALPHX,ALPHL,DELI,DELJ,RMASX,RMASL,XADP,DXX,DLX,EGA
      COMMON XND,XNA,XNO,XNSA,DELTU
      COMMON/ONE/ RHO,WL,Q14,ADP,CL,CT,EPSS,EPSO,REMAS,PAC,XNUM(25),
     C G(25),X,L,M
      CHARACTER ANS*3
C NUM=G(THETA/T), IS FORTINI*S FUNCTION
C INITIALIZATION
C L IS FLAG FOR ALGAAS OPTION
C M IS FLAG FOR TEMPERATURE RANGE OPTION
      EPSO=8.854E-12
C ENTERING ALL THE NECESSARY PARAMETERS
    1 WRITE (*,5)
    5 FORMAT (≠PLEASE ENTER ALL THE NECESSARY PARAMETERS FOR THIS MATERI
     CAL AND YOU ARE WELCOME TO THIS PROGRAM≠)
      PRINT*,*IT CALCULATES THE MOBILITIES IN TEMPERATURE RANGE OF 20 TO
     C 540 KELVIN*
   10 PRINT*,*ENTER THE PHONON TEMPERATURE OF THIS MATERIAL(THETA) IN DE
     CGREE KELVIN*,
   15 READ(*,*) THETA
   16 PRINT *,*DO YOU WANT TO CANCEL THETA VALUE, YES OR NO*,
      READ (*,*(A)*) ANS
      IF (ANS .NE. *YES* .AND. ANS .NE. *NO*) GO TO 16
      IF (ANS .EQ. *YES*) GO TO 10
      M=0
   21 PRINT*,*DO YOU WANT TO START FROM 20 TO 540, YES OR NO**,
      READ(*,*(A)*)ANS
      IF (ANS .NE. *YES* .AND. ANS .NE. *NO*) GO TO 21
      IF (ANS .EQ.*YES*) GO TO 23
      T(1) =50.0
      DO 22 I =1,18
        DT = 0.15 * T(I)
        T(I+1)= T(I)+DT
        G(I)=THETA/T(I)
   22 CONTINUE
      M=1
      GO TO 30
   23 T(1)=20.0
       PRINT   1000
1000  FORMAT(≠DATA READ≠)
      DO 24 I=1,25
        DT=0.15*T(I)
        T(I+1)= T(I) +DT
        G(I)= THETA/T(I)
   24 CONTINUE
   30 L=0
   33 PRINT*,*IS THIS FOR ALGAAS-YES OR NO*,
      READ(*,*(A)*)ANS
      IF (ANS .NE. *YES* .AND. ANS .NE. *NO*) GO TO 33
      IF (ANS .EQ. *YES*) THEN
         L=1
      ENDIF
```

```
   35 CALL ENTER
   36 PRINT*,*DO YOU WANT TO CANCEL THE PARAMETERS-YES/NO*,
      READ(*,*(A)*) ANS
      IF (ANS .NE. *YES* .AND. ANS .NE. *NO*) GO TO 36
      IF (ANS .EQ. *YES*) GO TO 35
C CALCULATIONS OF THE MOBILITIES
   40 CALL YENTR
   44 PRINT*,*DO YOU WANT TO CANCEL THE FITTING PARAMETERS-YES/NO*.
      READ(*,*(A)*) ANS
      IF (ANS .NE. *YES* .AND. ANS .NE. *NO*) GO TO 44
      IF (ANS .EQ. *YES*) GO TO 40
   42 WRITE(*,43)
   43 FORMAT (≠  TEMP.   ION.IMPR.   ALLOY SC.   DEFORM.P.   SP. CHAR.   PIEZO
     C ELC.   OPT.PHON.   UNI.MOBL.   TOT.MOBL.≠)
      IF (M .EQ. 1) THEN
         K=18
      ELSE
         K=25
      ENDIF
      XNN = XND + XNA
   45 DO 95 I=1,K
C CALCULATION OF THE B FACTOR
   50 B(I)=1.29E14*REMAS*EPSS*(T(I)**2)/(XND-XNA)
C CALCULATION OF THE IONIZED IMPURITY SCATTERING MOBILITY
   55 UI(I)=3.28E15*(EPSS**2)*(T(I)**1.5)/((2.*XNA+XND)
     C*(LOG(B(I)+1.)-(B(I)/(B(I)+1.)))*(REMAS**.5))
C CALCULATION OF OPTICAL PHONON MOBILITY
   60 UPO(I)=25.4*(T(I)**0.5)*(EXP(G(I))-1)*XNUM(I)/((1./EPSO-
     C1./EPSS)*(REMAS**1.5)*THETA)
C CALULATION OF THE ALLOY MOBILITY , STATEMENT 65 IS A DUMMY STATEMENT
   64 IF (L .EQ. 1) GO TO 67
   65 UA(I)=9.43E3/((T(I)**0.5)*(REMAS**2.5)*(DELTU**2)*(RAC**3))
   66 GO TO 70
C THIS IS ALLOY MOBILITY CALCULATION FOR ALGAAS
   67 UA(I)= 52.83/((T(I)**0.5)*(REMAS**2.5)*X*(1. -X)*(DELTU**2))
C CALCULATION OF THE DEFORMATION MOBILITY
   70 UDP(I)=(3.17E-5*RHO*(WL**2))/((T(I)**1.5)*(ADP**2)*(REMAS**2.5))
C CALCULATION OF THE PIEZOELECTRIC MOBILITY
   75 UPE(I)=2.52E12/((T(I)**0.5)*(REMAS**1.5)*((D14/(EPSS*
     CEPSO))**2)*((4./CT)+3./CL))
C CALCULATION OF SPACE CHARGE SCATTERING MOBILITY
   80 USC(I)=3.2E9/((T(I)**0.5)*(REMAS**0.5)*XNSA)
C  CALCULATION OF NEUTRAL IMPURITY SCATTERING MOBILITY (OAS)
   83 UNI(I) = ((1.17E22*REMAS)/(EPSS*8.859E-12*XNN)) *
     C  (7.34E-3*EPSS*8.859E-12*T(I)**0.5/REMAS**0.5 + 30.2*REMAS**
     C  0.5/(EPSS*8.859E-12*T(I)**0.5))
C CALCULATION OF THE TOTAL MOBILITY
   81 UTOT(I)=(1./UPE(I)+1./UPO(I)+1./USC(I)+1./UI(I)+1./UA(I)+
     C1./UDP(I) + 1./UNI(I))**(-1)
   85 WRITE(*,90)T(I),UI(I),UA(I),UDP(I),USC(I),UPE(I),UPO(I),UNI(I),
     C  UTOT(I)
   90 FORMAT (* *,F5.1,2X,E9.3,2X,E9.3,2X,E9.3,2X,E9.3,2X,E9.3,
     C 2X,E9.3,2X,E9.3,2X,E9.3)
 95         CONTINUE
         PRINT*,*              *
         WRITE(*,1122)
1122   FORMAT(≠ TEMP.   ION.IMPR.   ALLOY SC.   DEFORM.P.   SP.CHAR.   PIEZO
     CELC.   OPT.PHON.   UNI.MOBL.   EQ.VALL.   NONEQ.VALL.   UTOTX.≠)
            RMASL=0.14
            RMASX=0.35
            AADP=9.6
            DELI=0.03
            DELJ=0.05
```

```
          DXX=6.8E8
          DLX=9.25E8
            EGA=1.31E11*THETA
          ALPHX=(2.*DXX**2*WL**2)/(XADP**2*  EGA**2)
          ALPHL=(2.*DLX**2*WL**2)/(XADP**2*EGA**2)
1124   DO 96 I=1,K
C  CALCULATION OF B FACTOR FOR X VALLEY
200      BX(I)=1.29E14*RMASX*EPSS*(T(I)**2)/(XND-XNA)
C  CALCULATION OF IONIZED IMPURITY MOBILITY FOR X VALLEY
210      UIX(I)=3.28E15*(EPSS**2)*(T(I)**1.5)/((2.*XNA+XND)
     C   *(LOG(BX(I)+1.)-(BX(I)/(BX(I)+1.)))*(RMASX**.5))
C  CALCULATION OF OPTICAL PHONON MOBILITY FOR X VALLEY
220      UPOX(I)=25.4*(T(I)**0.5)*(EXP(G(I))-1)*XNUM(I)/
     C   ((1./EPSD-1./EPSS)*(RMASX**1.5)*THETA)
C  CALCULATION OF ALLOY MOBILITY FOR X VALLEY FOR ALGAAS
230      UAX(I)=52.83/((T(I)**0.5)*(RMASX**2.5)*X*(1.-X)
     C   *(DELTU**2))
C  CALCULATION OF DEFORMATION MOBILITY FOR X VALLEY
240      UDPX(I)=(3.17E-5*RHO*(WL**2))/((T(I)**1.5)*(XADP
     C   **2)*(RMASX**2.5))
C  CALCULATION OF PIEZOELECTRIC MOBILITY IN X VALLEY
250      UPEX(I)=2.52E12/((T(I)**0.5)*(RMASX**1.5)*
     C   ((Q14/(EPSS*EPSD))**2)*(4./CT+3./CL))
C  CALCULATION OF SPACE CHARGE MOBILITY IN X VALLEY
260      USCX(I)=3.2E9/((T(I)**0.5)*(RMASX**0.5)*XNSA)
C  CALCULATION OF NEUTRAL IMPURITY MOBILITY IN X VALLEY
270      UNIX(I)=((1.17E22*RMASX)/(EPSS*8.859E-12*XNN))*
     C   (7.34E-3*EPSS*8.859E-12*T(I)**0.5/RMASX**0.5
     C   +30.2*RMASX**0.5/(EPSS*8.859E-12*T(I)**0.5))
C  CALCULATION OF NONEQ. INT. VALLEY MOBILITY (LX)
         APPU(I)=(DELJ-DELI)/(8.625E-5*T(I))
         DEC(I)=1./G(I)-(2./3+APPU(I))
         IF (DEC(I)  .LE. 0 ) THEN
275      BLX(I)=0
       ELSE
276      BLX(I)=((1./G(I)-2./3+APPU(I))**0.5)/(1.-EXP(-G(I)))
       ENDIF
280      RLX(I)=(1./G(I)+2./3+APPU(I))**0.5/(EXP(G(I))-1)+BLX(I)
         ULX(I)=UDPX(I)*2.661/(RLX(I)*G(I)**1.5*ALPHL*3)
C  CALCULATION OF  EQ. INT. VALLEY MOBILITY  (XX)
         BEC(I)=1./G(I)-2./3
         IF (BEC(I) .LE. 0 )      THEN
285      BXX(I)=0
       ELSE
286      BXX(I)=(1./G(I)-2./3)**0.5/(1.-EXP(-G(I)))
       ENDIF
290      RXX(I)=(1/G(I)+2./3)**0.5/(EXP(G(I))-1)+BXX(I)
         UXX(I)=UDPX(I)*2.661/(RXX(I)*G(I)**1.5*ALPHX*3)
C  CALCULATION OF TOT. MOBILITY IN X VALLEY
300      UTOTX(I)=1./(1./UPEX(I)+1./UPOX(I)+1./USCX(I)+1./UIX(I)+
     C   1./UAX(I)+1./UDPX(I)+1./UNIX(I)+1./UXX(I)+1./ULX(I))
         WRITE(*,350) T(I),UIX(I),UAX(I),UDPX(I),USCX(I),UPEX(I),UPOX(I)
     C   ,UNIX(I),UXX(I),ULX(I),UTOTX(I)
350          FORMAT(F5.1,2X,10(E9.3,2X))
96     CONTINUE
          WRITE(*,1123)
1123      FORMAT(≠  TEMP.    UTOT.    UTOTX.      UTOTL.     UHALL    ≠)
        DO 97 I=1,K
C  SCALING UTOT FOR L VALLEY
400      UTOTL(I)=UTOT(I)/7.5
         RNL(I)=(RMASL/REMAS)**1.5*EXP(-DELJ/(8.625E-5*T(I)))
         RNX(I)=(RMASX/REMAS)**1.5*EXP(-DELI/(8.625E-5*T(I)))
         RUL(I)=UTOTL(I)/UTOT(I)
```

```
        RUX(I)=UTOTX(I)/UTOT(I)
        UAV(I)=1.+RNX(I)*RUX(I)+RNL(I)*RUL(I)
        UH(I)=UTOT(I)*(1.+RNX(I)*RUX(I)**2+RNL(I)*RUL(I)**2)/UAV(I)
500     WRITE(*,550) T(I),UTOT(I),UTOTX(I),UTOTL(I),UH(I),RNX(I),RNL(I)
550     FORMAT(F5.1,2X,6(E9.3,2X))
   97 CONTINUE
  100 PRINT*,*DO YOU WANT TO CHANGE THE MATERIAL - YES OR NO***,
  105 READ(*,*(A)*)ANS
  110 IF(ANS .NE.*YES* .AND. ANS.NE. *NO*) GO TO 100
  115 IF (ANS .EQ. *YES*) GO TO 10
  120 PRINT*,*DO YOU WANT TO CHANGE THE FITTING PARAMETERS-YES OR NO**,
  125 READ(*,*(A)*) ANS
  130 IF (ANS .NE.*YES* .AND. ANS .NE. *NO*) GO TO 120
  135 IF (ANS .EQ. *YES*)GO TO 40
  140 PRINT*,*THIS IS THE END OF THE PROGRAM, GOOD LUCK****
  145 STOP
  150 END
C THESE ARE THE SUBROUTINES TO ENTER THE DATA PARAMETERS
      SUBROUTINE ENTER
      COMMON/ONE/ RHO,WL,Q14,ADP,CL,CT,EPSS,EPSO,REMAS,RAD,XNUM(25),
     C G(25),X,L,M
      IF (M .EQ. 1) GO TO 4
      DO 3 I=1,25
        PRINT*,*ENTER THE VALUE OF G(THETA) FOR THETA/T=*,G(I)
        READ(*,*) XNUM(I)
    3   CONTINUE
      GO TO 10
    4 DO 5 I=1,18
        PRINT*,*ENTER THE VALUE OF G(THETA) FOR THETA/T=*,G(I)
        READ(*,*) XNUM(I)
    5 CONTINUE
   10 PRINT*,*ENTER THE MASS DENSITY IN GRAM PER  CM3*,
   15 READ(*,*) RHO
   20 PRINT*,*ENTER THE VELOCITY OF SOUND IN THAT MATERIAL IN CM PER SE
     CCOND*,
   25 READ(*,*) WL
   30 PRINT*,*ENTER THE PIEZOELECTRIC CONSTANT (E14) IN COULOMB PER M2
     C *,
   35 READ(*,*) Q14
   40 PRINT*,*ENTER THE ACOUSTIC DEFORMATION POTENTIAL IN ELECT.VOLT*,
   45 READ (*,*) ADP
   50 PRINT*,*ENTER THE RELATIVE EFFECTIVE MASS*,
   55 READ (*,*) REMAS
   60 PRINT*,*ENTER THE LONGITUDINAL ELASTIC CONSTANT IN DYNE/CM2*,
   65 READ (*,*) CL
   70 PRINT*, *ENTER THE TRANSVERSAL ELASTIC CONSTANT IN DYNE PER CM2*,
   75 READ (*,*) CT
   80 PRINT*, *ENTER THE LOW FREQUENCY DIELECTRIC CONSTANT,EPSS*,
   85 READ (*,*) EPSS
   90 PRINT*, *ENTER THE HIGH FREQUENCY DIELECTRIC CONSTANT,EPSO*,
   95 READ (*,*) EPSO
   99 IF (L .EQ. 1) GO TO 110
  100 PRINT *,*ENTER THE LATTICE CONSTANT IN ANGSTROMS*,
  105 READ (*,*) RAD
  106 GO TO 120
  110 PRINT *,*ENTER THE X VALUE OF AL GA AS*,
  115 READ (*,*)X
  120 RETURN
      END
C
C
      SUBROUTINE XENTR
      COMMON XND,XNA,XNO,XNSA,DELTU
```

```
 10 PRINT *, *ENTER ND IN CM-3*,
 20 READ (*,*) XND
 30 PRINT*, *ENTER NA PER CM3*,
 40 READ (*,*) XNA
 50 PRINT *, *ENTER NO PER CM3*,
 60 READ (*,*) XNO
 70 PRINT*, *ENTER THE ALLOYING POTENTIAL IN ELECTRON VOLTS*,
 80 READ (*,*) DELTU
 90 PRINT*,*ENTER NS.A IN CM-1*,
100 READ (*,*)XNSA
    RETURN
    END
```

Appendix III

Program for the Hall concentration analysis of $Al_xGa_{1-x}As$

```
      PROGRAM KARIM ( INPUT,OUTPUT)
      READ*,X
      READ*,GND1
      READ*,GND2
      READ*,GNA
      READ*,DED1
      READ*,DED2
      READ*,DEF
      READ*,T
      READ*,DEGL
      READ*,DEGX
      READ*,Y1
      READ*,U1
      READ*,V1
      READ*,UL
      READ*,UX
      READ*,UGAMA
      Z=GND1+GND2-GNA
      DO 100 I=1,20
      T=T+15
      BOLZT=(8.625E-5)*T
      EG=1.4206-4.906E-4*T**2/(T+327.)
      Y=Y1*T**1.5
      U=U1*T**1.5
      V=V1*T**1.5
   20 ODEF=DEF
      E=-DEF/BOLZT
      F=(-DED1+DEF)/BOLZT
      G=(-DED2+DEF)/BOLZT
      E2=-(DEF+DEGL+(6.E-5)*(T-300))/BOLZT
      E3=-(DEF+DEGX-(6.E-5)*(T-300))/BOLZT
C          A=NGAMA      AL1=NL         AX1=NX
      A=Y*EXP(E)
      AL1=U*EXP(E2)
      AX1=V*EXP(E3)
      B=GND1/(1.+0.5*EXP(F))
      C=GND2/(1.+0.5*EXP(G))
      P=A+AL1+AX1+B+C-Z
      AN=-(Y/BOLZT)*EXP(E)
      A2LN=-(U/BOLZT)*EXP(E2)
      A3XN=-(V/BOLZT)*EXP(E3)
      BN=-0.5*GND1*EXP(F)/(BOLZT*(1.+0.5*EXP(F)))**2
      CN=-0.5*GND2*EXP(G)/(BOLZT*(1.+0.5*EXP(G)))**2
      P1=AN+A2LN+A3XN+BN+CN
      DEF=DEF-P/P1
      IF(ABS(DEF-ODEF).GT.0.00001) GO TO 20
      EF=EG-DEF
      REVT=1.E3/T
      RUL=UL/UGAMA
      RUX=UX/UGAMA
      RASL=AL1/A
      RASX=AX1/A
      HALLN=A*(1.+RASL*RUL+RASX*RUX)/(1.+RASL*RUL**2+RASX*RUX**2)
      WRITE(*,33) REVT,T,A,AL1,AX1
      WRITE(*,43) DEF,EF,RUL,RUX,HALLN
  100 PRINT*,*          *
   33 FORMAT(2X,*REVT= *,F4.1,2X,*T= *,F5.1,2X,*A= *,E9.3,2X,
     C *AL1= *,E9.3,2X,*AX1= *,E9.3)
   43 FORMAT(2X,*DEF= *,F6.4,2X,*EF= *,F5.4,2X,*RUL= *,F4.2,2X,
     C *RUX= *,F4.2,2X,*HALLN= *,E9.3)
      END
```